Journal of Medicinal Chemistry Article

J. Med. Chem. **2009,** *52,* 6433–6446 **6433**
DOI: 10.1021/jm9009444

Structure-Based Optimization of Potent and Selective Inhibitors of the Tyrosine Kinase Erythropoietin Producing Human Hepatocellular Carcinoma Receptor B4 (EphB4)

Karine Lafleur,[†,‡] Danzhi Huang,[*,†] Ting Zhou,[†] Amedeo Caflisch,[*,†] and Cristina Nevado[*,‡]

[†]*Department of Biochemistry and* [‡]*Department of Organic Chemistry, University of Zurich, Winterthurerstrasse 190, CH-8057, Zurich, Switzerland*

Received June 26, 2009

The tyrosine kinase EphB4 is an attractive target for drug design because of its recognized role in cancer-related angiogenesis. Recently, a series of commercially available xanthine derivatives were identified as micromolar inhibitors of EphB4 by high-throughput fragment-based docking into the ATP-binding site of the kinase domain. Here, we have exploited the binding mode obtained by automatic docking for the optimization of these EphB4 inhibitors by chemical synthesis. Addition of only two heavy atoms, methyl and hydroxyl groups, to compound **4** has yielded the single-digit nanomolar inhibitor **66**, with a remarkable improvement of the ligand efficiency from 0.26 to 0.37 kcal/(mol per non-hydrogen atom). Compound **66** shows very high affinity for a few other tyrosine kinases with threonine as gatekeeper residue (Abl, Lck, and Src). On the other hand, it is selective against kinases with a larger gatekeeper. A 45 ns molecular dynamics (MD) simulation of the complex of EphB4 and compound **66** provides further validation of the binding mode obtained by fragment-based docking.

1. Introduction

Angiogenesis, the formation of new blood vessels from pre-existing ones, has been identified as one of the key steps in human carcinogenesis. In fact, nutrient supply and waste elimination are required for cell proliferation. Because of low toxicity and resistance potential,[1] as well as the possibility of treating a large spectrum of solid tumor types,[2] angiogenesis inhibition is considered a promising target in anticancer therapies. Several studies have implicated erythropoietin-producing human hepatocellular carcinoma receptor (Eph[a]) signaling in sprouting angiogenesis and blood vessel remodeling during vascular development.[3] Furthermore, overexpression of several of the 14 Eph receptors has been linked to tumors and the associated vasculature, suggesting a critical role in tumor-related angiogenesis. In fact, inhibition of binding of EphB4 to its natural ligand EphrinB2 using soluble extracellular domains of EphB4 has been shown to reduce tumor growth in murine tumor xenograft models.[4,5] Thus, inhibition of Eph angiogenic activity has been recognized as an effective strategy for blocking tumor progression and metastasis.

Like all receptor tyrosine kinases, EphB4 is a type-I transmembrane protein. Its extracellular domain is composed of an N-terminal domain necessary for ligand binding, whereas its intracellular domain includes a C-terminal domain and a tyrosine kinase domain. Despite the potential therapeutic importance of EphB4, only four series of small molecule inhibitors are currently known (Figure 1).[6−9] In 2007, Miyazaki and co-workers reported the synthesis of 3-[4-amino-3-(3-chloro-4-fluorophenyl)thieno-[3,2-*c*]pyridin-7-yl]-benzenesulfonamide (**1**), which is a potent EphB4 inhibitor.[7] One year later, 2,4-bis-anilinopyrimidine derivatives such as **2** showed also high potency as EphB4 inhibitors, and their cocrystallization with human EphB4 highlighted their dual binding mode (Figure 1).[10] The marketed drug dasatinib, with Abl1 and Src as primary targets, also showed a very high affinity to Eph kinases.[11]

High throughput docking is a computational tool frequently used to discover small-molecule inhibitors of enzymes or receptors of known three-dimensional structures.[12,13] Recently, we have developed an efficient computational method (termed ALTA for anchor-based library tailoring) to focus a chemical library by docking and prioritizing molecular fragments according to their binding energy.[6] From a collection of about 700 000 compounds, ALTA generated a focused library of 21 418 molecules, each containing at least one fragment predicted to bind to the ATP-binding site of EphB4. Automatic docking of these 21 418 molecules yielded two series of micromolar inhibitors, one of them based on a xanthine scaffold predicted to be involved in two hydrogen bonds with the hinge region that connects the N-terminal and C-terminal lobes of the kinase domain. Further characterization of the commercially available **3** (Figure 1) indicated that this molecule binds to the ATP-binding site, as predicted by the docking calculations.[6] In addition, an analogue with a pendent anisidine chain (**4**, Figure 1) showed similar inhibition properties to **3** and was active in a cell-based assay.

Here, we present a medicinal chemistry campaign aimed at improving the affinity of the micromolar hits **3** and **4** identified by in silico screening. The optimization was carried out using

*To whom correspondence should be addressed. For D.H.: phone, (41) 446355568; fax, (41) 446356862; e-mail, dhuang@bioc.uzh.ch. For A.C.: phone, (41) 446355521; fax, (41) 446356862; e-mail, caflisch@bioc.uzh.ch. For C.N.: phone, (41) 446353945; fax, (41) 446353948; e-mail, nevado@oci.uzh.ch.

[a] Abbreviations: Abl, Abelson murine leukemia viral oncogene homologue; ALTA, anchor-based library tailoring; ATP, adenosine triphosphate; DIPEA, diisopropylethylamine; DMF, dimethylformamide; DMSO, dimethyl sulfoxide; Eph, erythropoietin-producing human hepatocellular carcinoma receptor; FRET, fluorescence-resonance energy transfer; GCK, germinal center kinase; Lck, lymphocyte-specific kinase; MD, molecular dynamics; MLK, mixed-lineage kinase; rmsd, root-mean-square deviation; SAR, structure−activity relationship; THF, tetrahydrofuran.

Published on Web 09/29/2009

the binding mode obtained by automatic docking into EphB4. Chemical synthesis of about 30 derivatives of **3** and **4** yielded six nanomolar inhibitors, one of which (compound **66**) has an IC_{50} of 2−5 nM and shows good selectivity against other protein kinases. The addition of only two heavy atoms (−CH_3 and −OH substituents at the phenyl ring, **4** vs **66**) has resulted in a ∼1000 times improvement of affinity, which is a remarkable example of the usefulness of structure-based hit modifications.

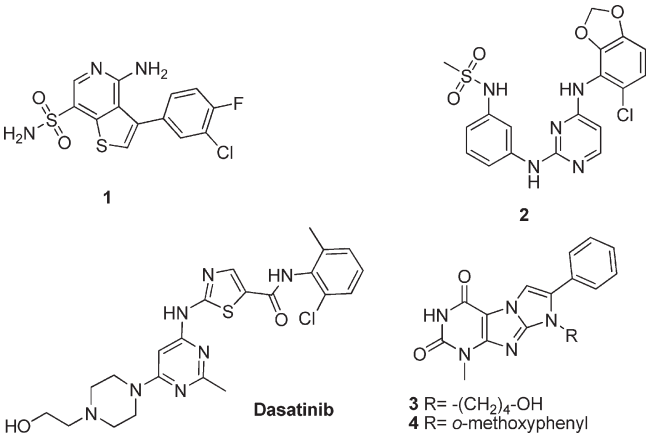

Figure 1. Previously known EphB4 inhibitors.[6−9]

2. Synthesis

Our foreseen modifications to the scaffold of compound **4** (R_{1-7}) for the structure−activity relationship study (SAR) have been summarized at the top of Table 1. Such studies demand a rapid, reliable, and flexible access to a wide variety of potentially active structures with a minimum synthetic variation cost. To succeed in such a goal, a modular synthetic approach was developed. Thus, methyl and benzyl substituted derivatives at R_1 were prepared in parallel as summarized in Scheme 1. The synthesis started by condensation of cyanoacetic acid with commercially available methylurea or benzylurea to give the corresponding cyanoacetylurea intermediates, which upon treatment with base afforded the desired 1-alkyl-6-aminouracils (**5**,**6**).[14] Nitrosation at C_5 of the pyrimidine ring with sodium nitrite in acetic acid furnished compounds **7** and **8**, which were subsequently reduced with sodium dithionite to give 1-alkyl-5,6-diaminouracils **9** and **10**.[15] The diamino compounds were immediately refluxed with formic acid to give an amide intermediate, followed by cyclization in basic media, to afford the desired xanthines **11** and **12**. Bromination at C_8 of the xanthine core with Br_2 and sodium acetate in acetic acid led to the formation of the key 8-bromoxanthines **13** and **14** in excellent overall yield.[16]

The synthesis of the noncommercially available α-halo ketones is summarized in Scheme 2. First, commercially available 1,3-benzodioxole-5-carboxaldehyde (piperonal, **15**)

Table 1. EphB4 Inhibition Data for Xanthine Derivatives

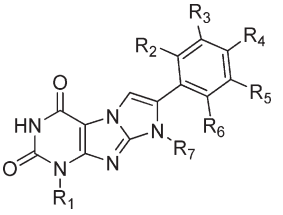

compd	R_1	R_2	R_3	R_4	R_5	R_6	R_7	IC_{50} (nM)[a]
3	Me	H	H	H	H	H	4-hydroxybutyl	7000 (5680)
4	Me	H	H	H	H	H	*o*-methoxyphenyl	3300 (4350)
45	Bn	H	H	H	H	H	*o*-methoxyphenyl	> 10000
46	Bn	H	H	F	H	H	*o*-methoxyphenyl	> 10000
69	H	H	H	F	H	H	*o*-methoxyphenyl	5400
48	Me	H	1,3-dioxol	H	H	H	*o*-methoxyphenyl	> 20000
49	Me	H	1,3-dioxol	H	H	H	4-hydroxybutyl	42% at 10 μM
50	Me	1,3-dioxol	H	H	H	H	*o*-methoxyphenyl	30% at 10 μM
51	Me	OMe	H	H	H	H	butyl	> 10000
52	Me	H	OMe	H	H	H	butyl	36% at 10 μM
53	Me	H	H	OMe	H	H	butyl	> 10000
54	Me	Me	H	H	H	H	*o*-methoxyphenyl	180 (47)
55	Me	H	Me	H	H	H	*o*-methoxyphenyl	> 10000
56	Me	H	Me	H	H	H	butyl	37% at 10 μM
57	Me	H	H	Me	H	H	butyl	38% at 10 μM
58	Me	OH	H	H	H	H	*o*-methoxyphenyl	64% at 10 μM
59	Me	OH	H	H	H	H	butyl	1600
60	Me	H	H	H	OH	H	*o*-methoxyphenyl	368 (213)
61	Me	H	H	H	OH	H	butyl	691
62	Me	H	H	OH	H	H	*o*-methoxyphenyl	59% at 10 μM
63	Me	H	H	OH	H	H	butyl	558
64	Me	Me	OH	H	H	H	*o*-methoxyphenyl	1200
65	Me	Me	H	OH	H	H	*o*-methoxyphenyl	236
66	Me	Me	H	H	OH	H	*o*-methoxyphenyl	5 (1.6)
67	Me	H	H	H	OH	OH	*o*-methoxyphenyl	5000

[a] IC_{50} values were measured by a FRET based enzymatic assay while values in parentheses are IC_{50} values determined by an enzymatic assay with radioactive ATP (see Experimental Section).

was reacted with methylmagnesium bromide to give secondary alcohol **16**, which was subsequently oxidized in the presence of manganese oxide to give methyl ketone **17**. α-Bromination at the methyl position took place in the presence of phenyltrimethylammonium tribromide to give alkylating agent **18** in only three steps. 2-Bromo-2′-methyl-3′-hydroxyacetophenone (**24**) and 2-bromo-2′-methyl-4′-hydroxyacetophenone (**25**) were prepared by treatment of the corresponding carboxylic acids with methyllithium to afford methyl ketones **21** and **23**, respectively (Scheme 2). Demethylation of **21** using $AlCl_3$ yielded phenolic derivative **22**. Finally, α-bromination at the methyl group was achieved in the presence of copper(II) bromide in chloroform to give monohalogenated ketones **24** and **25**.

Alkylation at the N_7 position of the xanthine core with the appropriate α-haloketone was accomplished using *N,N*-diisopropylethylamine in dimethylformamide, providing the 8-bromo-3-alkyl-7-(2-oxo-2-phenylethyl)xanthine derivatives **26**−**44** in good yields. Treatment of these intermediates with primary alkylamines or aromatic amines in a sealed tube at 180 °C in ethanol as solvent afforded the desired imidazo-[1,2-*f*]xanthine derivatives **45**−**68** (Scheme 3).

Two more derivatives were prepared as chemical probes to address the binding mode of these molecules to EphB4 (Scheme 4). First, the benzyl group in **46** was removed in the presence of Pd/C with ammonium formate to give **69**. Alternatively, the nitrile group in **68** was transformed into the corresponding carboxylic acid (**70**) by hydrolysis with sulfuric acid.

Scheme 1[a]

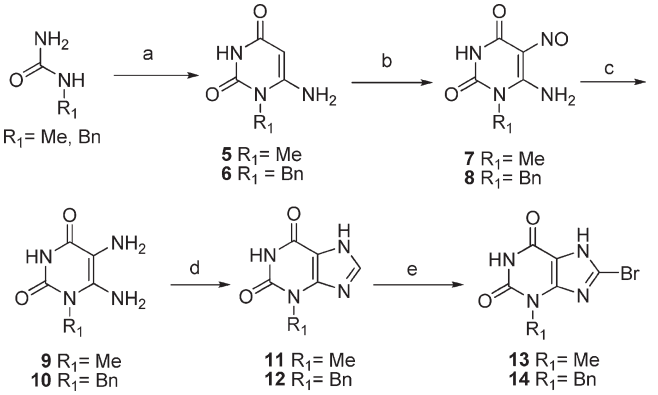

[a] Reagents and conditions: (a) (i) $NCCH_2CO_2H$, Ac_2O, 60 °C, 1.5 h; (ii) NaOH, 90 °C, 30 min; (b) $NaNO_2$, AcOH−H_2O, 25 °C, 12 h; (c) $Na_2S_2O_4$, NH_4OH, 50 °C, 1 h, then 25 °C, 8 h; (d) (i) formic acid, reflux, 3 h; (ii) NaOH, reflux, 1 h; (e) Br_2, NaOAc, AcOH, 65 °C, 2 h.

Scheme 2[a]

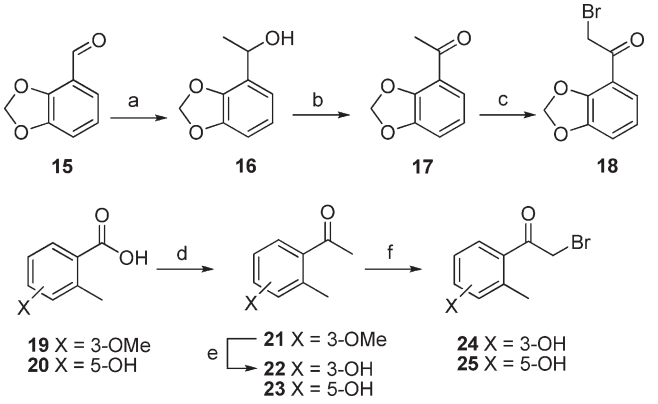

[a] Reagents and conditions: (a) MeMgBr, THF, −10 °C, 1 h; (b) MnO_2, Et_2O, 25 °C, 48 h; (c) phenyltrimethylammonium tribromide, THF, 25 °C, 16 h; (d) MeLi, Et_2O, 25 °C, 3.5 h; (e) $AlCl_3$, PhCl, reflux, 6 h; (f) $CuBr_2$, $CHCl_3$, EtOAc, reflux, 15 h.

3. Results and Discussion

The inhibitory activity of the compounds prepared in Schemes 3 and 4 was measured by a fluorescence resonance energy transfer (FRET) based enzymatic assay that quantifies inhibition of phosphorylation of a synthetic substrate of EphB4 at K_m concentration of ATP (see Experimental Section).

Experimental Validation of the Binding Mode. The binding mode of compound **3** obtained by automatic docking[6]

Scheme 4[a]

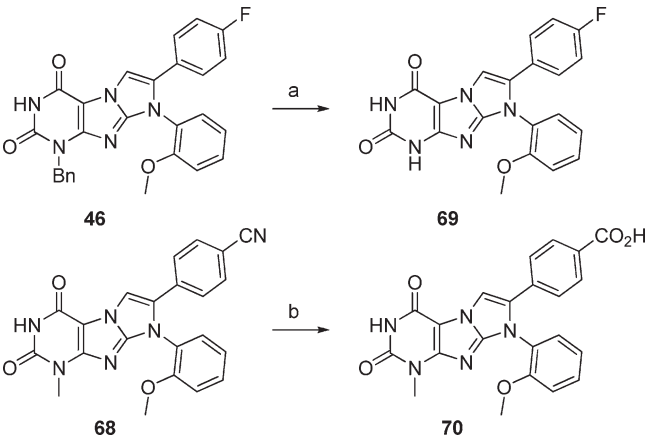

[a] Reagents and conditions: (a) Pd/C, ammonium formate, MeOH, 140 °C, 3 h; (b) H_2SO_4, H_2O, 120 °C, 2 h.

Scheme 3[a]

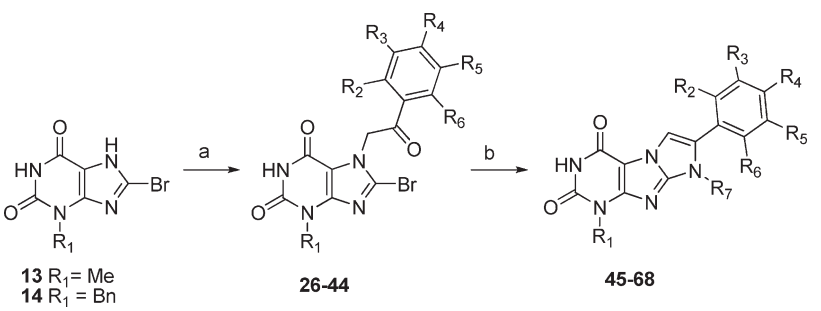

[a] Reagents and conditions: (a) α-halo ketone, DIPEA, DMF, 25 °C, 17 h; (b) primary amine, EtOH, sealed tube, reflux, 15 h.

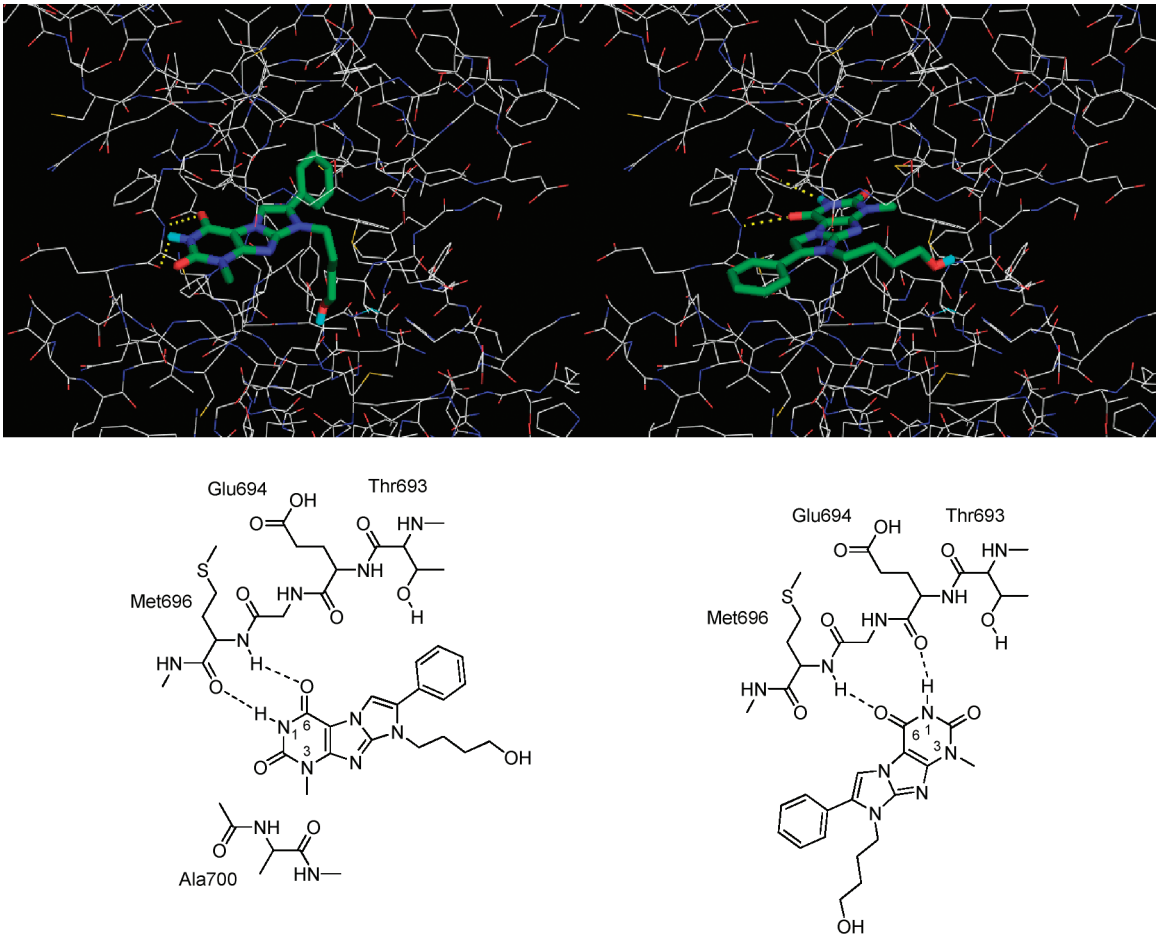

Figure 2. Binding modes of compound **3**. Poses A (left) and B (right) were generated by automatic[6] and manual docking, respectively. In the schematic view (bottom), the side chain of Phe695 is not shown for clarity.

Table 2. EphB4 Inhibition Data for Compounds Synthesized To Discriminate between Two Putative Binding Modes

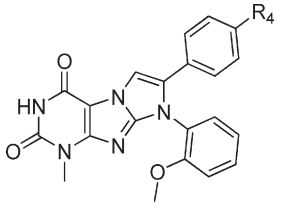

compd	R_4	IC_{50} (nM)
47	NO_2	> 20000
68	CN	> 20000
70	CO_2H	> 20000

indicated that the carbonyl C_6=O and amide group N_1−H are involved in hydrogen bonds with the backbone polar groups of Met696 (Figure 2, left). In this model, the phenyl ring of **3** is buried in the hydrophobic pocket, while the 4-hydroxybutyl lateral chain at R_7 points toward the solvent. Visual inspection of such binding mode suggested that another pose could be obtained by a 180° rotation of the first one (binding mode B, Figure 2, right) so that the phenyl ring points toward the solvent. In pose B, the C_6=O and N_1−H of compound **3** interact with the NH of Met696 and the backbone CO of Glu694, respectively. To discriminate between these two binding modes, we decided to introduce polar substituents at the para position of the phenyl ring. Derivatives with a nitro (**47**), a cyano (**68**), or a highly hydrophilic carboxylic group (**70**) were prepared according to the method described in Schemes 3 and 4. These three derivatives were inactive (Table 2). Furthermore, a hydroxyl substituent at R_4 reduced the affinity by a factor of about 2−3 (compare **4** and **62**, Table 1). These results indicate that the phenyl ring of compound **3** more likely fits into the hydrophobic pocket of the ATP-binding site, as suggested by automatic docking (binding mode A in Figure 2).

Lead Optimization Strategy. Once sufficient evidence about the binding mode had been gathered, we started our optimization campaign from commercially available **4** (compound **5** in ref 6). Compounds **3** and **4** differ only at R_7 (alkyl vs aromatic) and have similar IC_{50} values in the enzymatic assay (Table 1), but only the latter showed activity in a cell-based assay (Table 1 in ref 6). According to the binding mode, the substituent at N_3 of the pyrimidine ring could be involved in additional interactions with Ala700 (Figure 2) so that we decided to start the chemical edition of the molecule at R_1. The methyl group was replaced by a benzyl substituent, causing a major loss in the inhibitory activity of these molecules (**45** and **46** vs **4**). Compound **69**, with a N_3−H bond, was not more potent than **4**. Since no improvement was achieved by modification of the pyrimidine ring, we decided to focus our efforts on a different region of the molecule.

The ATP-binding site of protein kinases can be divided into five different subpockets.[17] The size of the hydrophobic pocket is controlled by a so-called gatekeeper residue, and it is well-known that not only affinity but also selectivity can be improved by fully exploring this site.[17] In fact, only around 20% of the 518 human kinases have a small gatekeeper residue. Since EphB4 belongs to this class having a threonine gatekeeper (Thr693), we envisioned that a straightforward strategy to improve affinity would stem from modifications of the substitution pattern at the phenyl ring. In sharp contrast to compound **2** and other previously developed inhibitors of EphB4,[8,10] a dioxole ring in relative positions R_3, R_4 (**48** and **49**) or R_2, R_3 (**50**) of the aromatic ring significantly reduced the activity. A methoxy group with different substitution patterns (**51**, **52**, **53**) also suppressed the inhibitory activity of the corresponding molecules. According to binding mode A (Figure 2), the space around the phenyl ring is rather limited, thus restricting the size of the substituents that might improve steric complementarity. Furthermore, the phenyl ring is close to the carbonyl group of Glu664, the hydroxyl and carbonyl groups of Ser757, and the NH group of Asp758, which can act as hydrogen bonding partners. On the basis of these observations, we decided to examine less sterically demanding substituents such as methyl or hydroxyl groups, which are expected to fulfill the nearby hydrogen bonding capacity.

Notably, a methyl substituent at position R_2 of the benzene ring (**54**) showed an IC_{50} value close to 100 nM. In contrast, R_3 and R_4 methyl substituted derivatives (**55**−**57**) were almost inactive. Furthermore, introduction of a hydroxyl group at R_5 (**60**) was also beneficial with an IC_{50} of about 200−400 nM. Some inhibition activity was also detected for compounds bearing the OH group at R_2 (**58**) and R_4 (**62**) of the phenyl ring. In these cases, replacing the anisidine lateral chain at R_7 (**58**, **60**, and **62**) for an alkyl one such as butyl (**59**, **61**, and **63**) seemed to have only a limited influence in the inhibitory activity of these molecules as previously observed for the commercially available compounds with a propyl or a butyl chain at R_7.[6] With these results in hand, we decided to explore how the combination of the most favored substitution patterns could influence the inhibitory activity. Thus, the methyl substituent was kept at R_2 and a hydroxyl group was added at the relative positions R_3 (**64**), R_4 (**65**), and R_5 (**66**) of the benzene ring. Strikingly, a combination of a methyl and a hydroxyl group at R_2 and R_5, respectively, yielded compound **66**, which has a ∼1000-fold higher affinity compared to the original hits obtained by docking, i.e., compounds **3** and **4**.

As mentioned above, the addition of only one heavy atom, CH_3 at R_2, resulted in a factor of 20−100 improvement (**54** vs **4**, or **66** vs **60**). This observation led us to further investigate the role of the methyl group, in particular if it stabilizes the orientation of the phenyl ring required for binding. Conformational analysis was performed on **4**, **54**, **60**, and **66** by exhaustive sampling of the dihedral angles involved in the rotation of the phenyl and *o*-methoxyphenyl rings (γ1 and γ2 in Figure S1 of the Supporting Information), followed by geometry optimization of the resulting structures using quantum mechanics. For each of the four inhibitors, the local minima are distributed into four sets of conformers, which are separated by rotation barriers. The docked conformation lies in one of these four basins whose local minima have similar energy values (maximal difference in energy of 0.082 kcal/mol for **4**, 0.219 kcal/mol for **54**, 0.257 kcal/mol for **60**, and 0.143 kcal/mol for **66**), which suggests a quasi-equal distribution of the population in each of the four conformers. Notably, the presence of a methyl group at R_2 seems to restrict the accessible conformations more than a hydroxyl group at R_5 (compare the plots obtained for **54** and **66** and for **4** and **60** in Figure S1). In addition, the conformational strain, which is the energy difference between the minimized bound conformation and the lowest energy conformation of the isolated ligand, was evaluated for each molecule. The similar values obtained for the strain energy of **54** (0.5 kcal/mol) and **4** (0 kcal/mol), as well as **66** (0.7 kcal/mol) and **60** (0.3 kcal/mol), indicate that the methyl group contributes to a gain in intermolecular van der Waals energy rather than in strain energy (see also the subsection Binding Mode of Compound **66** Investigated by MD Simulations).

Table 3. Local Selectivity of Compound **66**[a]

kinases	IC_{50} (nM)
EphA1	2.9
EphA2	2.3
EphA3	40
EphA4	3.3
EphA5	3.0
EphA7	1118
EphA8	4.5
EphB1	1.1
EphB2	1.2
EphB3	15
EphB4	1.6

[a] These IC_{50} values were measured at Reaction Biology Corporation.

During the preparation of this manuscript we discovered in the literature a series of inhibitors of the tyrosine kinase Lck with a 2,4-dianilinopyrimidine scaffold which have a very similar SAR for the phenyl substituents to the one observed for compounds **4**, **54**, **60**, and **66**.[18] Note that the phenyl substituent in both series of compounds is located in the hydrophobic pocket, but it is connected to the 2-anilinopyrimidine core by a −NH− linker in the Lck inhibitors whereas the phenyl ring is attached directly to the xanthine scaffold in the EphB4 inhibitors described here.

Selectivity Profile. To assess the specificity of kinase inhibitors, it is useful to distinguish between local and global selectivity profiles, which reflect the inhibitory activity of the tested compound on a single branch of the kinome dendrogram and on the whole kinome, respectively. The local selectivity of compound **66** was tested against a panel of 11 Eph receptor kinases by an enzymatic assay with [γ-^{33}P]ATP (Reaction Biology Corporation). The IC_{50} values measured for this compound against 10 of the 11 Ephs are in the low nanomolar range (1−40 nM), while an IC_{50} value of 1.1 μM is observed for EphA7 (Table 3). These IC_{50} values are consistent with the very high sequence identity (60−90%) of Ephs and the bulkier gatekeeper residue in EphA7 (isoleucine) with respect to the other Eph kinases (threonine). To evaluate the global selectivity, enzymatic assays (at single concentration of inhibitor) were performed for compounds **66** and **54** using a panel of 85 kinases (National Centre for Protein Kinase Profiling at the University of Dundee, Figure 3). Out of these 85 kinases, only five (EphA2, EphB3, Src, Lck, and Yes1) and three (EphA2, Lck, Yes1) are very strongly inhibited by compounds **66** and **54**, respectively (less than 10% activity remaining compared to a DMSO control at 1 μM of **66** and 3 μM of **54**; see Supporting Information). It is important to note that these

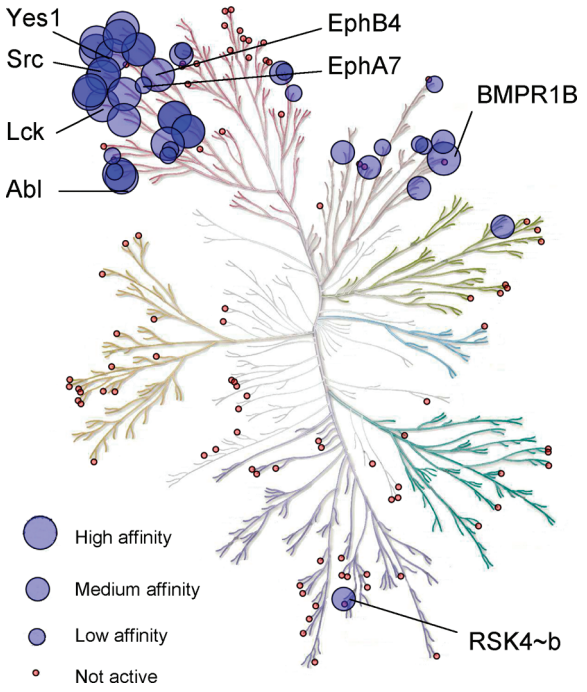

Figure 3. Selectivity profile of compound **66**. The circles correspond to all kinases tested. Inhibition of activity was measured in enzymatic assays with radiolabeled ATP at Reaction Biology Corporation and University of Dundee for 11 and 85 kinases, respectively, while binding affinity of 50 kinases was measured at Ambit Biosciences Corporation. Enzymatic assays: high, medium, low, and no compound affinity for kinase activity (with respect to DMSO control) of $<10\%$, $10-30\%$, $30-60\%$, and $>60\%$, respectively. Binding assay: high, medium, low, and no compound affinity for kinase activity (with respect to DMSO control) of $<1\%$, $1-10\%$, $10-30\%$, and $>30\%$, respectively. Kinome diagram is reproduced courtesy of Cell Signaling Technology, Inc. (www.cellsignal.com).[44]

five kinases have a threonine as gatekeeper, as well as CSK, BTK, and HER-4, which show relatively strong inhibition by **66** (between 10% and 50% activity remaining compared to a DMSO control).

The local and global selectivity profiles prompted us to test the binding of compound **66** against a set of 49 kinases (Ambit Biosciences Corporation) selected among the nearly 100 that are predicted to have a small gatekeeper based on sequence and structure analysis.[19] Interestingly, in competition binding assays, compound **66** shows significant affinity (kinase activity $<10\%$ with respect to DMSO control) to only 15 of these 49 kinases (see Supporting Information).

Considering all these selectivity tests (Figure 3), compound **66** has been profiled against a total of 143 kinases (three kinases, EphA2, EphB3, and EphB4, were tested twice) about half of which were chosen because of their small gatekeeper residue. Only 21 kinases with a threonine gatekeeper showed high inhibition by **66**, and 10 of them are Eph kinases (Figure 3). Among the kinases with a gatekeeper different from threonine, only GCK and MLK1 (both with methionine as a gatekeeper) are inhibited by compound **66**. Interestingly, the selectivity of **66** is consistent with the recently published kinase tree constructed by using SAR data,[20] as the kinases that bind compound **66** colocalize in a small branch of the SAR-based dendrogram (Abl, Src, and Eph families; see Supporting Information). Moreover, EphA7 is located in another branch of the SAR-based dendrogram, in agreement with the 100−1000 lower affinity with respect to the other 10 Eph kinases.

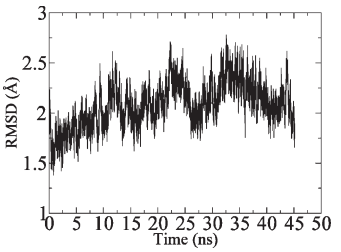

Figure 4. Time series of the Cα root-mean-square deviation (rmsd) of residues 613−883 of the kinase domain of EphB4 with respect to the X-ray structure (PDB code 2VWX). The loop 772−778 was not taken into account because it is not present in the crystal structure.

The profiles provide evidence for a good specificity of compound **66**, as it shows significant inhibition for a relatively small fraction of the human kinome, which is comparable to, or even more specific than some type I kinase inhibitors currently used as drugs, e.g., dasatinib[21] and sunitinib.[9] The high selectivity may originate from fully exploring the inner hydrophobic pocket whose size is controlled by the gatekeeper. In addition, the rigidity of this compound may contribute to its selectivity.

Binding Mode of Compound 66 Investigated by MD Simulations. Although the SAR of the 28 xanthine derivatives (Tables 1 and 2) is consistent with the pose of compounds **3** and **4** predicted by automatic docking,[6] explicit water molecular dynamics (MD) simulations were carried out to further validate the binding mode of compound **66**, which is the most potent of all derivatives. The MD run started from the pose of **66** obtained by automatic flexible ligand docking (see computational methods section). The structure of EphB4 is stable in the 45 ns simulation, as indicated by the time series of the Cα rmsd (Figure 4). Importantly, the hydrogen bonds with the hinge region (i.e., between the backbone polar groups of Met696 and the pyrimidine ring of compound **66**) are conserved during the entire run except for some transient ruptures of the one involving the carbonyl group of Met696 (Figure 5A,B). Furthermore, the side chain of Ser757 is involved in a rather stable hydrogen bond with the methoxy oxygen of compound **66** (Figure 5C). On the other hand, a change in the orientation of the hydroxyl group of compound **66** was observed after about 12 ns. The two hydrogen bonds with the side chain of Glu664 and the backbone NH of Asp758 broke apart with concomitant formation of a rather stable hydrogen bond with the backbone CO of Ser757 (Figure 5D). This change in the hydrogen bonding pattern of the hydroxyl group occurred immediately after the rotation of the peptide bond between Ser757 and Asp758 (Figure 5) and persisted until the end of the MD run. In other words, the reorientation of the Ser757 CO and Asp758 NH groups promoted the new hydrogen bond pattern.

Overall, the 45 ns MD simulation of the complex of EphB4 with compound **66** shows that the major features of the binding mode predicted by docking are stable. These include the orientation of the phenyl in the hydrophobic pocket and the two hydrogen bonds with the hinge region. It is interesting to note that **66** forms by its hydroxyl substituent one or two additional hydrogen bonds compared to compound **54**, which is consistent with its ∼30−35 higher affinity than that of **54** (Table 1). Furthermore, the methyl group at

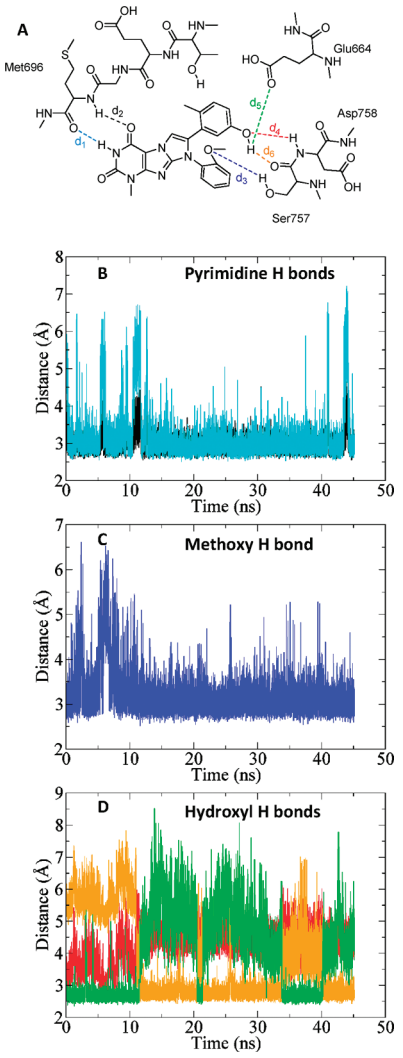

Figure 5. Hydrogen bonds between compound **66** and the ATP-binding site of EphB4: (A) schematic illustration; (B−D) time series of hydrogen-bond distances, i.e., the distance between the donor and acceptor atoms. The colors are consistent with those used in part A.

R_2 is involved in favorable van der Waals interactions with the side chains of Val629, Ala645, and Thr693 throughout the simulation (see Supporting Information). These van der Waals interactions contribute about −1.5 kcal/mol to the binding energy. Compounds **66** and **60** differ only by this methyl group so that the former has a more favorable desolvation energy upon binding, which, taken together with the additional van der Waals interactions with EphB4, explains the 100 times higher potency of compound **66** vs **60** (Table 1).

4. Conclusions

We had previously discovered a series of micromolar inhibitors of the tyrosine kinase EphB4 by fragment-based high-throughput docking of a library of about 700 000 compounds.[6] Here, we describe the structure-guided improvement of these relatively weak inhibitors by chemical synthesis which has culminated into the discovery of a single-digit nanomolar inhibitor **66**, with a remarkable increase in ligand efficiency[22] from 0.26 to 0.37 kcal/mol per non-hydrogen atom (for inhibitors **4** and **66**, respectively). Notably, compound **66** has only two non-hydrogen atoms more than **4** (a methyl group and a hydroxyl group on the same benzene ring), and these small but very effective substituents were suggested by analysis of the binding mode obtained by automatic docking. Furthermore, the predicted binding mode of compound **66** into the ATP-binding site of EphB4 is stable in a 45 ns MD simulation with explicit solvent. Analysis of the MD trajectory suggests that the higher potency of **66** with respect to **4** is due to favorable van der Waals interactions of the methyl group with the side chains of Val629, Ala645, and the gatekeeper residue (Thr693), as well as a hydrogen bond between the hydroxyl group and the backbone CO of Ser757. In addition, quantum mechanics calculations indicate that the beneficial effect of the methyl group is not due to a lower conformational strain upon binding but rather to the aforementioned van der Waals interactions. Although the SAR of all the compounds synthesized in this work is consistent with the binding mode of compound **66** obtained by docking and slightly refined by explicit solvent MD, its definitive validation awaits for X-ray crystallography, which is being pursued vigorously and will be reported in due course. Finally, compound **66** shows a relatively good selectivity profile, which is an important requirement for further consideration as a lead compound.

5. Experimental Section

Docking. The flexible ligand docking employed here for compounds **3** and **66** is a fragment-based approach, as it exploits the optimal binding modes of mainly rigid fragments. The approach consists of four consecutive steps which have been detailed in a previous work.[23] Briefly, the four steps are: (1) decomposition of the ligand into mainly rigid fragments by the program DAIM,[24] (2) fragment docking with evaluation of electrostatic solvation[25,26] by the program SEED,[27,28] (3) flexible docking using the position and orientation of its fragments as anchors by the program FFLD,[29,30] and (4) final minimization by CHARMM.[31,32] The protein structure (PDB file 2VWX) was kept rigid in all steps.

Parametrization of Compound 66 and MD Simulations. Initial Mulliken partial charges of 1,7,8-trimethyl-1*H*-imidazo[2,1-*f*]-purine-2,4(3*H*,8*H*)-dione were obtained by optimization with Gaussian 03 at the HF/6-31G(d) level.[33] Partial charges of hydrogen atoms in the methyl groups were set to 0.09*e*, and the excessive positive charge was added to the adjacent carbon atom. To determine the partial charges on the remaining atoms, interaction energies between each polar group and a TIP3 water molecule[34] were evaluated as the difference between the supermolecule energy and the sum of the individual monomer energies. The partial charges on the polar groups were then manually adjusted to fit the interaction energies calculated by CHARMM to the ab initio values. Bond lengths and angle values were also modified to reproduce the quantum mechanically obtained geometries. Normal mode contributions generated with the MOLVIB program were adjusted to scaled HF/6-31G(d) values. Final steps included introduction of the previously parametrized phenol and methyl moieties,[33] followed by optimization of the remaining missing parameters.

The coordinates of EphB4 were downloaded from the PDB database (2VWX). As the X-ray structure contains only residues 608−888, the $-COCH_3$ group and $-NHCH_3$ group were added to the N-terminal Lys608 and C-terminal Ala888, respectively. To reproduce neutral pH conditions, the side chains of aspartates and glutamates were negatively charged, those of lysines and arginines were positively charged, and histidines were considered neutral. The protein was immersed in an orthorhombic box of pre-equilibrated water molecules. The size of the box was chosen to have a minimal distance of 13 Å between the boundary and any atom of the protein. The program VMD[35]

was used for setting up the simulation system, while minimization, heating, and production runs were performed with NAMD[36] using the CHARMM22 force field[33] and the TIP3P model of water. Periodic boundary conditions were applied, and the particle-mesh Ewald approach[37] was used for the long-range electrostatics. The van der Waals interactions were truncated at a cutoff of 12 Å, and a switch function is applied starting at 10 Å. The MD simulation was performed at constant temperature of 310 K by applying the Langevin thermostat and at constant pressure of 1 atm using the Nose−Hoover Langevin piston pressure control.[38,39] The time step was 2 fs, and the SHAKE algorithm[40] was used to fix the length of covalent bonds involving hydrogen atoms. Coordinate sets were saved every 2 ps.

Evaluation of Strain Energy by Quantum Mechanics. Systematic rotation of rotatable bonds in increments of 10° and 20° for the two phenyls and the methoxy, respectively, was performed using CHARMM, and the resulting conformations were minimized with Gaussian 03 using the AM1 Hamiltonian. Removal of duplicate conformations was done using the Ultrafast Shape Recognition protocol[41] supplemented by a chirality descriptor that distinguishes molecules that are mirror images of each other. Geometry optimization of the resulting structures was done at the B3LYP level using the PC GAMESS version of the GAMESS quantum chemical package.[42] Redundant conformations were discarded by a second Shape Recognition analysis. The strain energy was calculated as the energy difference between the minimized bound conformation and the global minimum obtained by the systematic search.

Chemistry. All reactions, unless otherwise stated, were carried out under a nitrogen atmosphere using standard Schlenk techniques. All reagents were used as received unless otherwise noted. Solvents were purchased in the best quality available, degassed by purging thoroughly with nitrogen, and dried over activated molecular sieves of appropriate size. Alternatively, they were purged with argon and passed through alumina columns in a solvent purification system (Innovative Technology). Reactions were monitored by thin layer chromatography (TLC) using Merck TLC silica gel 60 F_{254}. Flash column chromatography was performed over silica gel (230−400 mesh). NMR spectra were recorded on a AV2 400 or AV2 500 MHz Bruker spectrometer. Chemical shifts are given in ppm. The spectra are calibrated to the residual ^{1}H and ^{13}C signals of the solvents. Multiplicities are abbreviated as follows: singlet (s), doublet (d), triplet (t), quartet (q), doublet−doublet (dd), quintet (quint), septet (sept), multiplet (m), and broad (br). Melting points were determined on a Buchi melting point B-540 instrument. Methylurea, benzylurea, benzo[*d*][1,3]dioxole-4-carbaldehyde (piperonal **15**), 2-methyl-3-methoxybenzoic acid (**19**), and 2-methyl-5-hydroxybenzoic acid (**20**) were purchased from Fluka. The following compounds 2-bromo-1-phenylethanone, 2-bromo-1-(4-fluorophenyl)ethanone, 2-bromo-1-(4-methoxyphenyl)ethanone, 2-bromo-1-(3-methoxyphenyl)ethanone, 2-bromo-1-(2-methoxyphenyl)ethanone, 2-chloro-1-(4-hydroxyphenyl)ethanone, 2-bromo-1-(3-hydroxy.phenyl)ethanone, 2-bromo-1-(2-hydroxyphenyl)-ethanone, 2-chloro-1-(3,4-dihydroxyphenyl)ethanone, 2-bromo-1-(4-nitrophenyl)ethanone, 2-bromo-4′-cyanoacetophenone, 2-chloro-1-(4-hydroxy-2-methylphenyl)ethanone, and 2-bromo-1-(4-methylphenyl)-1-ethanone were purchased from Fluka. 2-Bromo-1-(3-methylphenyl)-1-ethanone and 2-bromo-1-(2-methylphenyl)-1-ethanone were purchased from Synchem, and 1-(1,3-benzodioxol-5-yl)-2-bromo-1-ethanone was purchased from Acros Organics.

High-resolution electrospray ionization mass spectrometry was performed on a Finnigan MAT 900 (Thermo Finnigan, San Jose, CA) double-focusing magnetic sector mass spectrometer. Ten spectra were acquired. A mass accuracy of ≤2 ppm was obtained in the peak matching acquisition mode by using a solution containing 2 μL of PEG200, 2 μL of PPG450, and 1.5 mg of NaOAc (all obtained from Sigma-Aldrich, Buchs, Switzerland) dissolved in 100 mL of MeOH (HPLC Supra grade, Scharlau, E-Barcelona, Spain) as internal standard. The purity of all tested compounds was determined by HPLC on a Finnigan Voyager GC8000 Top spectrometer using an Interchim Strategy (2.2 μm, 2.1 mm × 100 mm) column by running a 5−80% gradient for water (+0.1% HCOOH + 0.01% TFA)/CH_3CN. Flow rate was 200 μL/min, and UV detection was set to 254 nm. Unless otherwise stated, all the compounds showed ≥95% purity.

1-(Benzo[*d*][1,3]dioxol-4-yl)ethanol (16).[43] A solution of MeMgBr in THF (1 M, 9.9 mL, 9.9 mmol, 1.5 equiv) was diluted with THF (10 mL) and cooled to −10 °C. A solution of benzo[*d*][1,3]dioxole-4-carbaldehyde **15** (1.0 g, 6.6 mmol) in 9.9 mL of THF was slowly added, and the mixture was stirred for 1 h. The reaction mixture was then quenched by pouring it into 100 mL of ice cold saturated ammonium chloride, and the aqueous layer was then extracted with Et_2O. The organic extracts were dried over $MgSO_4$ and evaporated under reduced pressure to provide the desired compound as a colorless oil (971 mg, 88% yield). ^{1}H NMR (400 MHz, $CDCl_3$): δ = 6.87 (ddd, J = 7.8, 1.4, 0.4 Hz, 1H), 6.82 (dd, J = 7.8, 7.5 Hz, 1H), 6.75 (dd, J = 7.5, 1.4 Hz, 1H), 5.96 (d, J = 1.4 Hz, 1H), 5.95 (d, J = 1.4 Hz, 1H), 4.99 (q, J = 6.5 Hz, 1H), 1.52 (d, J = 6.5 Hz, 3H), OH not observed. ^{13}C NMR (100 MHz, $CDCl_3$): δ = 147.3, 143.9, 127.3, 121.7, 118.7, 107.7, 100.8, 66.2, 23.3. IR (film): $\tilde{\nu}$ = 3359, 2972, 2887, 1455, 1245, 1039, 727 cm^{-1}. MS (ESI), m/z: calcd for $C_9H_{10}NaO_3$, 189.1; found, 189.0 $[M + Na]^+$.

1-(Benzo[*d*][1,3]dioxol-4-yl)ethanone (17).[43] A mixture of 1-(benzo[*d*][1,3]dioxol-4-yl)ethanol **16** (971 mg, 5.84 mmol) and MnO_2 (5.08 g, 58.4 mmol) in Et_2O (36 mL) was stirred vigorously for 48 h. The reaction mixture was then filtered through a path of Celite and evaporated under reduced pressure to give the desired compound as a white solid (679 mg, 70% yield). Mp 95−97 °C. ^{1}H NMR (400 MHz, $CDCl_3$): δ = 7.37 (dd, J = 8.2, 1.3 Hz, 1H), 6.97 (dd, J = 7.6, 1.3 Hz, 1H), 6.87 (dd, J = 8.2, 7.6 Hz, 1H), 6.09 (s, 2H), 2.60 (s, 3H). ^{13}C NMR (100 MHz, $CDCl_3$): δ = 195.4, 148.6, 147.9, 121.4, 121.2, 120.3, 112.5, 101.5, 30.2. IR (film): $\tilde{\nu}$ = 3068, 2908, 1671, 1625, 1450, 1361, 1283, 1240, 1179, 1060, 1022, 950, 727 cm^{-1}. MS (EI), m/z: calcd for $C_9H_8O_3$, 164.1; found, 163.9 $[M]^+$.

1-(Benzo[*d*][1,3]dioxol-4-yl)-2-bromoethanone (18).[43] To a solution of 1-(benzo[*d*][1,3]dioxol-4-yl)ethanone **17** (679 mg, 4.14 mmol) in anhydrous THF (19 mL) at 0 °C was added phenyltrimethylammonium tribromide (1.55 g, 4.14 mmol). The reaction mixture was stirred at room temperature for 16 h, concentrated, and redissolved in EtOAc. The organic layer was washed with water (2 × 50 mL) and brine (1 × 50 mL), dried over $MgSO_4$, filtered, and evaporated under reduced pressure. Purification by column chromatography on silica gel (toluene/hexane, 1:4), followed by recrystallization in hexane/EtOAc afforded the desired compound as a white solid (309 mg, 30% yield). Mp 75−77 °C. ^{1}H NMR (500 MHz, $CDCl_3$): δ = 7.42 (dd, J = 8.2, 1.2 Hz, 1H), 7.01 (dd, J = 7.6, 1.2 Hz, 1H), 6.91 (dd, J = 8.2, 7.6 Hz, 1H), 6.11 (s, 2H), 4.48 (s, 2H). ^{13}C NMR (125 MHz, $CDCl_3$): δ = 188.2, 148.5, 147.8, 121.9, 121.7, 117.1, 113.3, 101.8, 34.9. IR (film): $\tilde{\nu}$ = 3002, 2942, 2917, 1693, 1624, 1451, 1387, 1248, 1204, 1177, 1048, 942, 768, 723 cm^{-1}. MS (ESI), m/z: calcd for $C_9H_7BrNaO_3$, 264.9; found, 265.0 $[M + Na]^+$.

1-(3-Methoxy-2-methylphenyl)ethanone (21). To a solution of 2-methyl-3-methoxybenzoic acid **19** (1.5 g, 9.02 mmol) in dry diethyl ether (68 mL) at 0 °C, methyllithium (1.6 M in Et_2O, 22 mL, 36.1 mmol) was added dropwise with vigorous stirring. The mixture was allowed to warm to room temperature and stirred for an additional 3.5 h. The reaction was quenched by pouring the mixture into ice cold 10% HCl (50 mL), and the aqueous layer was then extracted with Et_2O (3 × 50 mL). The organic solution was washed with brine, dried over $MgSO_4$, filtered, and concentrated under reduced pressure. Purification by column chromatography on silica gel (hexane/EtOAc, 16:1) afforded the desired compound as a colorless oil (613 mg, 41%). ^{1}H NMR (500 MHz, $CDCl_3$): δ = 7.22 (dd, J = 8.1, 7.6 Hz, 1H),

7.15 (dd, J = 7.6, 1.1 Hz, 1H), 6.95 (d, J = 8.1 Hz, 1H), 3.85 (s, 3H), 2.55 (s, 3H), 2.32 (s, 3H). ^{13}C NMR (125 MHz, $CDCl_3$): δ = 203.1, 158.2, 140.6, 126.1, 125.9, 120.0, 112.7, 55.8, 30.4, 12.6. IR (film): $\tilde{\nu}$ = 3001, 2960, 2938, 2836, 1684, 1577, 1456, 1258, 1051, 781 cm^{-1}. MS (ESI), m/z: calcd for $C_{10}H_{12}NaO_2$, 187.1; found, 187.0 $[M + Na]^+$.

1-(3-Hydroxy-2-methylphenyl)ethanone (22). A solution of 1-(3-methoxy-2-methylphenyl)ethanone **21** (450 mg, 2.74 mmol) in chlorobenzene (11 mL) was treated with $AlCl_3$ (475 mg, 3.56 mmol) at room temperature and then refluxed for 5 h. A second portion of $AlCl_3$ (475 mg, 3.56 mmol) was added, and the resulting mixture was refluxed for an additional hour until no starting material was detected by TLC. The reaction mixture was carefully treated with 1 M HCl at 0 °C. The aqueous phase was extracted with EtOAc, and the combined organic layers were dried with $MgSO_4$. Evaporation of the solvent and column chromatography on silica gel (hexane/EtOAc, 6:1) afforded the desired compound as a yellow solid (328 mg, 79% yield). Mp 122−124 °C. ^{1}H NMR (400 MHz, $CDCl_3$): δ = 7.18 (dd, J = 7.8, 1.2 Hz, 1H), 7.12 (t, J = 7.8 Hz, 1H), 6.93 (dd, J = 7.8, 1.2 Hz, 1H), 5.34 (s, 1H), 2.57 (s, 3H), 2.36 (s, 3H). ^{13}C NMR (100 MHz, $CDCl_3$): δ = 203.4, 154.7, 140.4, 126.2, 123.3, 120.9, 118.0, 30.1, 12.4. IR (film): $\tilde{\nu}$ = 3221, 1652, 1577, 1466, 1360, 1277, 782 cm^{-1}. MS (ESI), m/z: calcd for $C_9H_{10}NaO_2$, 173.1; found, 173.0 $[M + Na]^+$.

1-(5-Hydroxy-2-methylphenyl)ethanone (23). To a solution of 2-methyl-5-hydroxybenzoic acid **20** (900 mg, 5.9 mmol) in THF (6.5 mL) at −78 °C was added MeLi (1.6 M in ether, 11 mL, 17.7 mmol). The mixture was stirred for 17 h while slowly warming up to room temperature. EtOAc (10 mL) was slowly added to the reaction mixture, which was subsequently washed (10 mL of 1 M HCl, 10 mL of water, and 10 mL of brine). After drying of the organic layer over $MgSO_4$ and evaporation of the solvent under reduced pressure, the residue was purified by flash chromatography on silica gel (EtOAc/hexane, 1:10) to afford desired compound as a white solid (608 mg, 68% yield). Mp 129−131 °C. ^{1}H NMR (400 MHz, $CDCl_3$): δ = 7.17 (d, J = 2.6 Hz, 1H), 7.10 (d, J = 8.2 Hz, 1H), 6.88 (dd, J = 8.2, 2.6 Hz, 1H), 5.32−5.37 (m, 1H), 2.55 (s, 3H), 2.43 (s, 3H). ^{13}C NMR (100 MHz, $CDCl_3$): δ = 201.9, 153.4, 138.5, 133.1, 130.2, 118.7, 116.1, 29.5, 20.6. IR (film): $\tilde{\nu}$ = 3188, 2929, 1657, 1603, 1456, 1434, 1302, 1221, 734 cm^{-1}. MS (ESI), m/z: calcd for $C_9H_{10}NaO_2$, 173.1; found, 173.0 $[M + Na]^+$.

General Procedure for the α-Bromination of Acetophenones. A solution of acetophenone (1 equiv) in $CHCl_3$ (0.18 M) was added to a refluxing solution of copper(II) bromide (1.99 equiv) in EtOAc (0.45 M). The mixture was then refluxed for 10 h. The solution was filtered through Celite and concentrated under reduced pressure to afford a green solid. The solid was purified by flash chromatography on silica gel (toluene) to afford the corresponding products in pure form. This method was used to obtain **24** and **25**.

2-Bromo-1-(3-hydroxy-2-methylphenyl)ethanone (24). White solid. Yield: 61%. ^{1}H NMR (400 MHz, $CDCl_3$): δ = 7.15−7.17 (m, 2H), 6.95−6.98 (m, 1H), 5.14 (s, 1H), 4.39 (s, 2H), 2.34 (s, 3H). ^{13}C NMR (100 MHz, $CDCl_3$): δ = 195.1, 154.7, 137.2, 126.5, 124.4, 120.6, 118.8, 34.2, 12.4. IR (film): $\tilde{\nu}$ = 3420, 2933, 1683, 1581, 1466, 1327, 796 cm^{-1}. MS (ESI), m/z: calcd for $C_9H_9BrNaO_2$, 250.9; found, 251.0 $[M + Na]^+$.

2-Bromo-1-(5-hydroxy-2-methylphenyl)ethanone (25). White solid. Yield: 50%. Mp 63−65 °C. ^{1}H NMR (400 MHz, $CDCl_3$): δ = 7.14−7.16 (m, 2H), 6.91 (dd, J = 8.2, 2.7 Hz, 1H), 4.92 (s, 1H), 4.37 (s, 2H), 2.43 (s, 3H). ^{13}C NMR (100 MHz, $CDCl_3$): δ = 194.1, 153.3, 135.4, 133.4, 131.5 119.4, 115.7, 33.5, 20.3. IR (film): $\tilde{\nu}$ = 3232, 2962, 2924, 1662, 1562, 1492, 1294, 1198, 824, 632 cm^{-1}. MS (GC/MS), m/z: calcd for $C_9H_{10}BrO_2$, 230.1; found, 230.2 $[M + H]^+$.

General Method for the Preparation of Alkylated Xanthines 26−40, 42, 44. 3-Alkyl-8-bromoxanthine (0.55 mmol) was dissolved in anhydrous DMF (4 mL), and distilled *N*,*N*-diisopropylethylamine (1.5 equiv) was added. After the mixture was stirred for 5 min at room temperature, α-bromoacetophenone (1 equiv) was slowly added. The mixture was stirred at room temperature for 1−3 days. The mixture was then poured into EtOAc/HCl (10%), and the formed precipitate was filtered and washed with water to afford **26−42** in pure form.

3-Benzyl-8-bromo-3,7-dihydro-7-(2-oxo-2-phenylethyl)-1*H*-purine-2,6-dione (26). White solid. Yield: 76%. Mp 249−252 °C. ^{1}H NMR (500 MHz, DMSO-d_6): δ = 11.43 (s, 1H), 8.10 (d, J = 7.4 Hz, 2H), 7.77 (t, J = 7.4 Hz, 1H), 7.63 (t, J = 7.4 Hz, 2H), 7.27−7.38 (m, 5H), 5.94 (s, 2H), 5.11 (s, 2H). ^{13}C NMR (125 MHz, DMSO-d_6): δ = 191.2, 153.9, 150.2, 148.5, 136.5, 134.5, 133.5, 129.2, 129.0, 128.4, 128.2, 127.3, 127.3, 109.0, 52.9, 44.9. IR (film): $\tilde{\nu}$ = 3190, 3059, 2978, 2936, 1707, 1697, 1669, 1592, 1536, 1446, 1358, 1260, 742 cm^{-1}. HRMS (ESI), m/z: calcd for $C_{20}H_{16}BrN_4O_3$, 439.0; found, 439.1 $[M + H]^+$.

3-Benzyl-8-bromo-7-[2-(4-fluorophenyl)-2-oxoethyl]-3,7-dihydro-1*H*-purine-2,6-dione (27). White solid. Yield: 62%. Mp 258−261 °C. ^{1}H NMR (500 MHz, DMSO-d_6): δ = 11.43 (s, 1H), 8.18−8.22 (m, 2H), 7.45−7.49 (m, 2H), 7.27−7.38 (m, 5H), 5.93 (s, 2H), 5.11 (s, 2H). ^{13}C NMR (125 MHz, DMSO-d_6): δ = 189.9, 153.9, 150.2, 148.6, 136.5, 131.4 (d, J = 9.8 Hz), 130.3 (d, J = 2.7 Hz), 129.2, 128.4, 127.5, 127.3, 127.3, 116.1 (d, J = 22.1 Hz), 109.0, 52.8, 44.9. IR (film): $\tilde{\nu}$ = 3184, 3068, 2972, 2934, 1697, 1665, 1592, 1536, 1359, 1234, 834, 742 cm^{-1}. HRMS (ESI), m/z: calcd for $C_{20}H_{14}BrFN_4NaO_3$, 479.0131; found, 479.0137 $[M + Na]^+$.

8-Bromo-3,7-dihydro-3-methyl-7-[2-(4-nitrophenyl)-2-oxoethyl]-1*H*-purine-2,6-dione (28). Yellow solid. Yield: 63%. Mp 290−292 °C. ^{1}H NMR (500 MHz, DMSO-d_6): δ = 11.32 (s, 1H), 8.42 (d, J = 8.9 Hz, 2H), 8.34 (d, J = 8.9 Hz, 2H), 6.01 (s, 2H), 3.37 (s, 3H). ^{13}C NMR (125 MHz, DMSO-d_6): δ = 190.9, 153.9, 150.6, 150.4, 149.0, 138.2, 129.8, 129.0, 124.0, 108.8, 53.2, 28.5. IR (film): $\tilde{\nu}$ = 3158, 3037, 2939, 2831, 1674, 1523, 1369, 1346, 1220, 1203, 852 cm^{-1}. HRMS (ESI), m/z: calcd for $C_{14}H_{11}BrN_5O_5$, 407.9; found, 408.1 $[M + H]^+$.

7-[2-(Benzo[*d*][1,3]dioxol-5-yl)-2-oxoethyl]-8-bromo-3,7-dihydro-3-methyl-1*H*-purine-2,6(3*H*,7*H*)-dione (29). White solid. Yield: 61%. Mp 297−299 °C. ^{1}H NMR (500 MHz, DMSO-d_6): δ = 11.23 (s, 1H), 7.76 (dd, J = 8.2, 1.5 Hz, 1H), 7.56 (d, J = 1.5 Hz, 1H), 7.13 (d, J = 8.2 Hz, 1H), 6.19 (s, 2H), 5.83 (s, 2H), 3.37 (s, 3H). ^{13}C NMR (100 MHz, DMSO-d_6): δ = 189.0, 153.9, 152.5, 150.4, 148.9, 148.1, 129.1, 127.9, 125.0, 108.9, 108.4, 107.3, 102.3, 52.6, 28.5. IR (film): $\tilde{\nu}$ = 3155, 3039, 2942, 2811, 1674, 1447, 1357, 1258, 1035, 930, 869, 817 cm^{-1}. HRMS (ESI), m/z: calcd for $C_{15}H_{11}BrN_4NaO_5$, 428.9811; found, 428.9808 $[M + Na]^+$.

7-[2-(Benzo[*d*][1,3]dioxol-4-yl)-2-oxoethyl]-8-bromo-3,7-dihydro-3-methyl-1*H*-purine-2,6-dione (30). White solid. Yield: 67%. Mp 306−308 °C. ^{1}H NMR (500 MHz, DMSO-d_6): δ = 11.31 (s, 1H), 7.35 (d, J = 7.9 Hz, 1H), 7.27 (d, J = 7.9 Hz, 1H), 7.02 (t, J = 7.9 Hz, 1H), 6.28 (s, 2H), 5.69 (s, 2H), 3.36 (s, 3H). ^{13}C NMR (125 MHz, DMSO-d_6): δ = 188.1, 153.9, 150.4, 148.9, 148.7, 148.4, 129.0, 122.0, 119.9, 115.9, 113.6, 108.9, 102.4, 55.0, 28.5. IR (film): $\tilde{\nu}$ = 3170, 3057, 2831, 1680, 1454, 1352, 1235, 1064, 946,745 cm^{-1}. HRMS (ESI), m/z: calcd for $C_{15}H_{11}BrN_4NaO_5$, 428.9811; found, 428.9808 $[M + Na]^+$.

8-Bromo-3,7-dihydro-7-[2-(2-methoxyphenyl)-2-oxoethyl]-3-methyl-1*H*-purine-2,6-dione (31). White solid. Yield: 75%. Mp 294−296 °C. ^{1}H NMR (500 MHz, DMSO-d_6): δ = 11.29 (s, 1H), 7.78 (d, J = 7.4 Hz, 1H), 7.69 (t, J = 7.4 Hz, 1H), 7.30 (d, J = 7.4 Hz, 1H), 7.12 (t, J = 7.4 Hz, 1H), 5.68 (s, 2H), 4.02 (s, 3H), 3.36 (s, 3H). ^{13}C NMR (125 MHz, DMSO-d_6): δ = 191.1, 159.6, 153.9, 150.4, 148.9, 135.9, 130.2, 129.0, 123.2, 120.8, 112.8, 108.8, 56.4, 56.1, 28.5. IR (film): $\tilde{\nu}$ = 3170, 2987, 2900, 1673, 1462, 1357, 1204, 758 cm^{-1}. HRMS (ESI), m/z: calcd for $C_{15}H_{13}BrN_4NaO_4$: 415.0018; found, 415.0019 $[M + Na]^+$.

8-Bromo-3,7-dihydro-7-[2-(3-methoxyphenyl)-2-oxoethyl]-3-methyl-1*H*-purine-2,6-dione (32). White solid. Yield: 75%. Mp 263−265 °C. ^{1}H NMR (400 MHz, DMSO-d_6): δ = 11.30 (s, 1H), 7.71 (ddd, J = 7.7, 1.5, 0.9 Hz, 1H), 7.57 (dd, J = 2.6, 1.5 Hz, 1H), 7.54 (dd, J = 8.1, 7.7 Hz, 1H), 7.33 (ddd, J = 8.1, 2.6, 0.9 Hz, 1H), 5.92 (s, 2H), 3.86 (s, 3H), 3.37 (s, 3H). ^{13}C NMR

(100 MHz, DMSO-d_6): δ = 191.0, 159.5, 153.9, 150.4, 148.9, 134.8, 130.2, 129.1, 120.7, 120.6, 112.5, 108.9, 55.4, 53.0, 28.5. IR (film): $\tilde{\nu}$ = 3145, 3027, 2807, 1679, 1535, 1365, 1261, 748 cm^{-1}. HRMS (ESI), *m*/*z*: calcd for $C_{15}H_{13}BrN_4NaO_4$, 415.0018; found, 415.0018 $[M + Na]^+$.

8-Bromo-3,7-dihydro-7-[2-(4-methoxyphenyl)-2-oxoethyl]-3-methyl-1*H*-purine-2,6-dione (33). White solid. Yield: 73%. Mp 280−282 °C. ^{1}H NMR (500 MHz, DMSO-d_6): δ = 11.29 (s, 1H), 8.08 (d, *J* = 8.9 Hz, 2H), 7.13 (d, *J* = 8.9 Hz, 2H), 5.86 (s, 2H), 3.88 (s, 3H), 3.37 (s, 3H). ^{13}C NMR (125 MHz, DMSO-d_6): δ = 189.2, 164.1, 153.9, 150.4, 148.9, 130.6, 129.1, 126.4, 114.3, 108.9, 55.6, 52.5, 28.5. IR (film): $\tilde{\nu}$ = 3153, 3034, 2941, 2838, 1680, 1600, 1364, 1173, 834 cm^{-1}. MS (ESI), *m*/*z*: calcd for $C_{15}H_{14}BrN_4O_4$, 393.2; found, 393.1 $[M + H]^+$.

8-Bromo-3,7-dihydro-3-methyl-7-[2-(2-methylphenyl)-2-oxoethyl]-1*H*-purine-2,6-dione (34). White solid. Yield: 58%. Mp 242−244 °C. ^{1}H NMR (500 MHz, DMSO-d_6): δ = 11.32 (s, 1H), 8.04 (dd, *J* = 7.6, 1.1 Hz, 1H), 7.56 (dt, *J* = 7.6, 1.1 Hz, 1H), 7.44 (t, *J* = 7.6 Hz, 1H), 7.40 (d, *J* = 7.6 Hz, 1H), 5.79 (s, 2H), 3.37 (s, 3H), 2.42 (s, 3H). ^{13}C NMR (125 MHz, DMSO-d_6): δ = 194.1, 153.9, 150.4, 148.9, 138.3, 133.7, 132.7, 131.9, 129.1, 129.0, 126.1, 108.8, 54.3, 28.5, 20.6. IR (film): $\tilde{\nu}$ = 3154, 3025, 2814, 1676, 1535, 1364, 1208, 768 cm^{-1}. HRMS (ESI), *m*/*z*: calcd for $C_{15}H_{13}BrN_4NaO_3$, 399.0069; found, 399.0068 $[M + Na]^+$.

8-Bromo-3,7-dihydro-3-methyl-7-[2-(3-methylphenyl)-2-oxoethyl]-1*H*-purine-2,6-dione (35). White solid. Yield: 75%. Mp 280−282 °C. ^{1}H NMR (500 MHz, DMSO-d_6): δ = 11.30 (s, 1H), 7.93 (s, 1H), 7.90 (d, *J* = 7.6 Hz, 1H), 7.58 (d, *J* = 7.6 Hz, 1H), 7.51 (t, *J* = 7.6 Hz, 1H), 5.91 (s, 2H), 3.37 (s, 3H), 2.42 (s, 3H). ^{13}C NMR (125 MHz, DMSO-d_6): δ = 191.2, 153.9, 150.4, 148.9, 138.6, 135.1, 133.5, 129.1, 128.9, 128.5, 125.3, 108.9, 52.9, 28.5, 20.7. IR (film): $\tilde{\nu}$ = 3149, 3024, 2813, 1678, 1536, 1360, 1164, 715 cm^{-1}. HRMS (ESI), *m*/*z*: calcd for $C_{15}H_{13}BrN_4NaO_3$, 399.0069; found, 399.0070 $[M + Na]^+$.

8-Bromo-3,7-dihydro-3-methyl-7-[2-(4-methylphenyl)-2-oxoethyl]-1*H*-purine-2,6-dione (36). White solid. Yield: 68%. Mp 293−295 °C. ^{1}H NMR (500 MHz, DMSO-d_6): δ = 11.29 (s, 1H), 8.00 (d, *J* = 7.8 Hz, 2H), 7.43 (d, *J* = 7.8 Hz, 2H), 5.89 (s, 2H), 3.37 (s, 3H), 2.42 (s, 3H). ^{13}C NMR (125 MHz, DMSO-d_6): δ = 190.6, 153.9, 150.4, 148.9, 145.2, 131.0, 129.5, 129.1, 128.2, 108.9, 52.7, 28.5, 21.2. IR (film): $\tilde{\nu}$ = 3155, 3002, 2819, 1677, 1538, 1369, 1203, 751 cm^{-1}. MS (ESI), *m*/*z*: calcd for $C_{15}H_{14}BrN_4O_3$, 377.0; found, 377.1 $[M + H]^+$.

8-Bromo-3,7-dihydro-7-[2-(2-hydroxyphenyl)-2-oxoethyl]-3-methyl-1*H*-purine-2,6-dione (37). White solid. Yield: 48%. Mp 289−291 °C. ^{1}H NMR (400 MHz, DMSO-d_6): δ = 11.28 (s, 1H), 11.19 (s, 1H), 7.80 (dd, *J* = 7.9, 1.8 Hz, 1H), 7.55 (ddd, *J* = 8.3, 7.2, 1.8 Hz, 1H), 7.08 (dd, *J* = 8.3, 0.9 Hz, 1H), 6.98 (ddd, *J* = 7.9, 7.2, 0.9 Hz, 1H), 5.76 (s, 2H), 3.37 (s, 3H). ^{13}C NMR (100 MHz, DMSO-d_6): δ = 191.8, 159.2, 153.9, 150.4, 148.9, 136.1, 130.0, 129.1, 120.5, 119.5, 117.5, 108.9, 55.8, 28.5. IR (film): $\tilde{\nu}$ = 3150, 3034, 2807, 1680, 1535, 1366, 1208, 748 cm^{-1}. HRMS (ESI), *m*/*z*: calcd for $C_{14}H_{11}BrN_4NaO_4$, 400.9861; found, 400.9856 $[M + Na]^+$.

8-Bromo-3,7-dihydro-7-[2-(3-hydroxyphenyl)-2-oxoethyl]-3-methyl-1*H*-purine-2,6-dione (38). White solid. Yield: 75%. Mp 299−305 °C. ^{1}H NMR (400 MHz, DMSO-d_6): δ = 11.30 (s, 1H), 9.97 (s, 1H), 7.57 (d, *J* = 8.1 Hz, 1H), 7.39−7.44 (m, 2H), 7.15 (ddd, *J* = 8.1, 2.5, 0.7 Hz, 1H), 5.86 (s, 2H), 3.37 (s, 3H). ^{13}C NMR (100 MHz, DMSO-d_6): δ = 191.0, 157.8, 153.9, 150.4, 148.9, 134.8, 130.2, 129.1, 121.6, 119.1, 114.1, 108.9, 52.9, 28.5. IR (film): $\tilde{\nu}$ = 3370, 3008, 2822, 1676, 1534, 1364, 1209, 750 cm^{-1}. HRMS (ESI), *m*/*z*: calcd for $C_{14}H_{11}BrN_4NaO_4$, 400.9861; found, 400.9860 $[M + Na]^+$.

8-Bromo-3,7-dihydro-7-[2-(4-hydroxyphenyl)-2-oxoethyl]-3-methyl-1*H*-purine-2,6-dione (39). Yellow solid. Yield: 74%. Mp 320−322 °C. ^{1}H NMR (500 MHz, DMSO-d_6): δ = 11.28 (s, 1H), 10.64 (s, 1H), 7.97 (d, *J* = 8.6 Hz, 2H), 6.93 (d, *J* = 8.6 Hz, 2H), 5.81 (s, 2H), 3.36 (s, 3H). ^{13}C NMR (125 MHz, DMSO-d_6): δ = 188.8, 163.2, 153.9, 150.4, 148.9, 130.8, 129.2, 125.0, 115.6, 108.9, 52.4, 28.5. IR (film): $\tilde{\nu}$ = 3154, 2818, 1680, 1577, 1360, 1208, 1166, 759 cm^{-1}. HRMS (ESI), *m*/*z*: calcd for $C_{14}H_{11}BrN_4NaO_4$, 400.9861; found, 400.9858 $[M + Na]^+$.

8-Bromo-3,7-dihydro-3-methyl-7-[2-(2-methyl-3-hydroxyphenyl)-2-oxoethyl]-1*H*-purine-2,6-dione (40). White solid. Yield: 72%. Mp 277−279 °C. ^{1}H NMR (400 MHz, DMSO-d_6): δ = 11.32 (s, 1H), 9.80 (s, 1H), 7.37 (dd, *J* = 7.8, 0.8 Hz, 1H), 7.22 (t, *J* = 7.8 Hz, 1H), 7.07 (dd, *J* = 7.8, 0.8 Hz, 1H), 5.70 (s, 2H), 3.36 (s, 3H), 2.18 (s, 3H). ^{13}C NMR (100 MHz, DMSO-d_6): δ = 195.1, 156.1, 153.9, 150.4, 148.9, 136.0, 129.0, 126.4, 123.6, 118.9, 118.6, 108.8, 54.7, 28.5, 12.2. IR (film): $\tilde{\nu}$ = 3411, 3145, 3023, 2823, 1663, 1535, 1366, 1274, 1205, 785 cm^{-1}. HRMS (ESI), *m*/*z*: calcd $C_{15}H_{13}BrN_4NaO_4$, 415.0018; found, 415.0011 $[M + Na]^+$.

8-Bromo-3,7-dihydro-3-methyl-7-[2-(2-methyl-5-hydroxyphenyl)-2-oxoethyl]-1*H*-purine-2,6-dione (42). White solid. Yield: 35%. Mp 271−274 °C. ^{1}H NMR (400 MHz, DMSO-d_6): δ = 11.32 (s, 1H), 9.73 (s, 1H), 7.34 (d, *J* = 2.6 Hz, 1H), 7.17 (d, *J* = 8.3 Hz, 1H), 6.96 (dd, *J* = 2.6, 8.3 Hz, 1H), 5.71 (s, 2H), 3.37 (s, 3H), 2.29 (s, 3H). ^{13}C NMR (100 MHz, DMSO-d_6): δ = 194.1, 155.3, 153.9, 150.4, 148.9, 134.5, 132.9, 129.1, 127.9, 119.6, 115.4, 108.8, 54.3, 28.5, 19.6. IR (film): $\tilde{\nu}$ = 3370, 3145, 3025, 2829, 1677, 1535, 1365, 1293, 1183, 749 cm^{-1}. HRMS (ESI), *m*/*z*: calcd for $C_{15}H_{13}BrN_4NaO_4$, 415.0018; found, 415.0007 $[M + Na]^+$.

8-Bromo-7-[2-(4-cyanophenyl)-2-oxoethyl]-3,7-dihydro-3-methyl-1*H*-purine-2,6-dione (44). White solid. Yield: 79%. Mp 281−284 °C. ^{1}H NMR (500 MHz, DMSO-d_6): δ = 11.31 (s, 1H), 8.25 (d, *J* = 8.5 Hz, 2H), 8.11 (d, *J* = 8.5 Hz, 2H), 5.98 (s, 2H), 3.36 (s, 3H). ^{13}C NMR (125 MHz, DMSO-d_6): δ = 191.1, 153.9, 150.4, 149.0, 136.7, 132.9, 129.0, 128.9, 117.9, 116.3, 108.8, 53.1, 28.5. IR (film): $\tilde{\nu}$ = 3162, 3043, 2963, 2932, 1705, 1671, 1540, 1369, 1204, 834 cm^{-1}. HRMS (ESI), *m*/*z*: calcd for $C_{15}H_{11}BrN_5O_3$, 388.0; found, 388.0 $[M + H]^+$.

8-Bromo-3,7-dihydro-3-methyl-7-[2-(2-methyl-4-hydroxyphenyl)-2-oxoethyl]-1*H*-purine-2,6-dione (41). 8-Bromo-3,9-dihydro-3-methyl-1*H*-purine-2,6-dione (**13**, 400 mg, 1.41 mmol) was added to a solution of KOH (79 mg, 1.41 mmol) in EtOH (3 mL). The resulting mixture was then heated to reflux for 2 h. EtOH was then removed under reduced pressure, and the resulting solid was washed with cold EtOH and filtered off to afford a light-yellow solid. A mixture of this solid (250 mg, 0.88 mmol) and α-bromo-4-hydroxy-2-methylacetophenone (202 mg, 0.88 mmol) in anhydrous DMF (2.5 mL) was stirred at room temperature for 16 h. The mixture was then poured into EtOAc/HCl (10%), and the formed precipitate was filtrated off and washed with water to afford the desired product as a white solid (177 mg, 51% yield). Mp 313−315 °C. ^{1}H NMR (400 MHz, DMSO-d_6): δ = 11.28 (s, 1H), 10.45 (s, 1H), 8.00 (d, *J* = 8.6 Hz, 1H), 6.78 (dd, *J* = 8.6, 2.4 Hz, 1H), 6.73 (d, *J* = 2.4 Hz, 1H), 5.73 (s, 2H), 3.36 (s, 3H), 2.39 (s, 3H). ^{13}C NMR (100 MHz, DMSO-d_6): δ = 190.6, 161.6, 153.9, 150.4, 148.9, 142.6, 132.6, 129.2, 124.2, 118.9, 112.8, 108.9, 53.6, 28.5, 21.8. IR (film): $\tilde{\nu}$ = 3225, 3145, 3025, 2987, 1673, 1540, 1371, 1204, 1065, 743 cm^{-1}. HRMS (ESI), *m*/*z*: calcd for $C_{15}H_{13}BrN_4NaO_4$, 415.0018; found, 415.0015 $[M + Na]^+$.

8-Bromo-7-[2-(3,4-dihydroxyphenyl)-2-oxoethyl]-3,7-dihydro-3-methyl-1*H*-purine-2,6-dione (43). 8-Bromo-3,9-dihydro-3-methyl-1*H*-purine-2,6-dione (**13**, 500 mg, 2.04 mmol) was dissolved in anhydrous DMF (5 mL), and distilled diisopropylethylamine (0.534 mL, 3.06 mmol) was added. After the mixture was stirred at 5 min at room temperature, α-chloro-3,4-dihydroxyacetophenone (380 mg, 2.04 mmol) was slowly added. The reaction mixture was heated to 70 °C for 5 h. The mixture was then poured into EtOAc/HCl (10%), and the organic layer was concentrated under reduced pressure. The resulting suspension was filtered and washed with MeOH to afford the desired product as a white solid (294 mg, 36% yield). Mp 311−314 °C. ^{1}H NMR (400 MHz, DMSO-d_6): δ = 11.29 (s, 1H), 10.16 (s, 1H), 9.52 (s, 1H), 7.53 (dd, *J* = 8.2, 1.9 Hz, 1H), 7.40 (d, *J* = 1.9 Hz, 1H), 6.90 (d, *J* = 8.2 Hz, 1H), 5.77 (s, 2H), 3.36 (s, 3H). ^{13}C NMR (100 MHz, DMSO-d_6): δ = 188.8, 153.9, 151.9, 150.4, 148.9, 145.6, 129.2, 125.3, 121.7,

115.3, 114.7, 108.9, 52.3, 28.5. IR (film): $\tilde{\nu}$ = 3460, 3233, 3044, 2945, 1698, 1666, 1357, 1289, 1186, 1065, 763 cm^{-1}. HRMS (ESI), *m*/*z*: calcd for $C_{14}H_{11}BrN_4NaO_5$, 416.9808; found, 416.9805 [M + Na]$^+$.

General Method for the Cyclization of Alkylated Xanthines 45−50, 54, 55, 58, 60, 62, 64−68. A mixture of 3-alkyl-8-bromo-3,7-dihydro-7-(2-oxo-2-phenyl-ethyl)-1*H*-purine-2,6-dione (1.0 equiv) and the corresponding primary amine (4.0 equiv) in EtOH (0.1 M) was heated in a sealed tube at 175 °C for 12 h. The mixture was cooled to room temperature and the solid was filtered off and washed with water, affording the corresponding products in pure form. This method was used to obtain compounds **45**−**50**, **54**, **55**, **58**, **60**, **62**, **64**−**68**.

General Method for the Cyclization of Alkylated Xanthines 51−53, 56, 57, 59, 61, 63. A mixture of 3-alkyl-8-bromo-3,7-dihydro-7-(2-oxo-2-phenylethyl)-1*H*-purine-2,6-dione (1.0 equiv) and butylamine (4.0 equiv) in *n*-PrOH (0.1 M) was heated in a sealed tube at 175 °C for 12 h. The mixture was cooled to room temperature, and the solid was filtered off and washed with water. Subsequent recrystallization in EtOH afforded the corresponding products in pure form. This method was used to obtain compounds **51**−**53**, **56**, **57**, **59**, **61**, **63**.

1-Benzyl-8-(2-methoxyphenyl)-7-phenyl-1*H*-imidazo[2,1-*f*]-purine-2,4(3*H*,8*H*)-dione (45). White solid. Yield: 40%. Mp 301−303 °C. ^{1}H NMR (400 MHz, DMSO-d_6): δ = 11.08 (s, 1H), 8.00 (s, 1H), 7.46−7.50 (m, 2H), 7.23−7.29 (m, 10H), 7.18 (d, *J* = 7.8 Hz, 1H), 7.06 (t, *J* = 7.8 Hz, 1H), 5.06 (s, 2H), 3.54 (s, 3H). ^{13}C NMR (100 MHz, DMSO-d_6, $CDCl_3$): δ = 154.7, 153.3, 152.4, 150.6, 147.8, 136.9, 132.9, 131.1, 129.5, 128.3, 128.2, 128.1, 127.5, 127.1, 127.1, 122.4, 120.9, 113.0, 105.4, 99.1, 55.6, 44.9, 1C missing due to overlapping. IR (film): $\tilde{\nu}$ = 3151, 3030, 2817, 1669, 1488, 1263, 1155, 1024, 754, 529 cm^{-1}. HRMS (ESI), *m*/*z*: calcd for $C_{27}H_{21}N_5NaO_3$, 486.1542; found, 486.1540 [M + Na]$^+$.

1-Benzyl-7-*p*-fluorophenyl-8-(2-methoxyphenyl)-1*H*-imidazo-[2,1-*f*]purine-2,4(3*H*,8*H*)-dione (46). White solid. Yield: 19%. Mp 251−253 °C. ^{1}H NMR (500 MHz, DMSO-d_6): δ = 11.09 (s, 1H), 7.99 (s, 1H), 7.46−7.49 (m, 2H), 7.25−7.29 (m, 6H), 7.20−7.23 (m, 1H), 7.12−7.17 (m, 3H), 7.04−7.08 (m, 1H), 5.05 (s, 2H), 3.54 (s, 3H). ^{13}C NMR (125 MHz, DMSO-d_6): δ = 161.9 (d, *J* = 246.7 Hz), 154.7, 153.4, 152.4, 150.7, 147.8, 136.9, 132.0, 131.3, 129.9 (d, *J* = 8.4 Hz), 129.6, 128.3, 127.1, 127.1, 124.6 (d, *J* = 3.1 Hz), 122.2, 121.0, 115.4 (d, *J* = 21.8 Hz), 113.1, 105.6, 99.1, 55.7, 44.9. IR (film): $\tilde{\nu}$ = 3160, 3025, 2822, 1671, 1487, 1225, 1157, 841, 744, 529, 409 cm^{-1}. MS (ESI), *m*/*z*: calcd for $C_{27}H_{20}FN_5NaO_3$, 504.4; found, 505.0 [M + Na]$^+$.

8-(2-Methoxyphenyl)-1-methyl-7-*p*-nitrophenyl-1*H*-imidazo-[2,1-*f*]purine-2,4(3*H*,8*H*)-dione (47). Yellow solid. Yield: 63%. Mp 323−325 °C. ^{1}H NMR (400 MHz, DMSO-d_6): δ = 11.06 (s, 1H), 8.35 (s, 1H), 8.14 (d, *J* = 8.7 Hz, 2H), 7.64 (dd, *J* = 7.6, 1.1 Hz, 1H), 7.55 (dt, *J* = 7.6, 1.1 Hz, 1H), 7.51 (d, *J* = 8.7 Hz, 2H), 7.21 (d, *J* = 7.6 Hz, 1H), 7.16 (t, *J* = 7.6 Hz, 1H), 3.54 (s, 3H), 3.30 (s, 3H). ^{13}C NMR (100 MHz, DMSO-d_6): δ = 154.4, 153.3, 153.2, 150.9, 148.4, 146.5, 134.8, 131.5, 130.8, 129.5, 127.7, 123.6, 122.1, 121.2, 113.1, 107.6, 99.2, 55.7, 28.8. IR (film): $\tilde{\nu}$ = 3012, 2826, 1680, 1501, 1016, 844, 720, 600, 432 cm^{-1}. HRMS (ESI), *m*/*z*: calcd for $C_{21}H_{16}N_6NaO_5$, 455.1080; found, 455.1085 [M + Na]$^+$.

7-(Benzo[*d*][1,3]dioxol-5-yl)-8-(2-methoxyphenyl)-1-methyl-1*H*-imidazo[1,2-*f*]purine-2,4(3*H*,8*H*)-dione (48). White solid. Yield: 33%. Mp 323−328 °C. ^{1}H NMR (400 MHz, DMSO-d_6): δ = 10.97 (s, 1H), 7.90 (s, 1H), 7.50−7.54 (m, 2H), 7.20 (dd, *J* = 8.9, 1.2 Hz, 1H), 7.10 (ddd, *J* = 8.8, 7.7, 1.2 Hz, 1H), 6.82−6.84 (m, 2H), 6.71 (dd, *J* = 8.1, 1.8 Hz, 1H), 6.00 (s, 2H), 3.62 (s, 3H), 3.29 (s, 3H). ^{13}C NMR (125 MHz, DMSO-d_6): δ = 154.9, 153.3, 152.7, 150.9, 147.8, 147.4, 147.1, 132.8, 131.3, 129.9, 122.5, 121.7, 121.6, 120.9, 112.9, 108.2, 107.9, 104.9, 101.2, 99.0, 55.7, 28.8. IR (film): $\tilde{\nu}$ = 3142, 3007, 2820, 1674, 1484, 1448, 1235, 1024, 737 cm^{-1}. HRMS (ESI), *m*/*z*: calcd for $C_{22}H_{17}N_5NaO_5$, 454.1127; found, 454.1125 [M + Na]$^+$.

7-(Benzo[*d*][1,3]dioxol-5-yl)-8-(4-hydroxybutyl)-1-methyl-1*H*-imidazo[1,2-*f*]purine-2,4(3*H*,8*H*)-dione (49). White solid. Yield: 12%. Mp 267−270 °C. ^{1}H NMR (400 MHz, DMSO-d_6): δ = 10.85 (s, 1H), 7.61 (s, 1H), 7.16−7.17 (m, 1H), 7.05−7.06 (m, 2H), 6.12 (s, 2H), 4.35 (s, 1H), 4.09 (t, *J* = 7.4 Hz, 2H), 3.40 (s, 3H), 3.26 (t, *J* = 7.4 Hz, 2H), 1.67 (quint, *J* = 7.4 Hz, 2H), 1.24 (quint, *J* = 7.4 Hz, 2H). ^{13}C NMR (100 MHz, DMSO-d_6): δ = 153.2, 152.7, 150.9, 147.9, 147.7, 147.6, 131.9, 123.1, 121.4, 109.3, 108.6, 104.8, 101.5, 98.8, 59.8, 43.6, 29.1, 28.8, 25.0. IR (film): $\tilde{\nu}$ = 3575, 3369, 3161, 3012, 2936, 2822, 1676, 1498, 1451, 1243, 1028, 742 cm^{-1}. HRMS (ESI), *m*/*z*: calcd for $C_{19}H_{19}N_5NaO_5$, 420.1284; found, 420.1289 [M + Na]$^+$.

7-(Benzo[*d*][1,3]dioxol-4-yl)-8-(2-methoxyphenyl)-1-methyl-1*H*-imidazo[1,2-*f*]purine-2,4(3*H*,8*H*)-dione (50). White solid. Yield: 38%. Mp 347−349 °C. ^{1}H NMR (500 MHz, DMSO-d_6): δ = 11.01 (s, 1H), 7.87 (s, 1H), 7.51−7.53 (m, 2H), 7.20 (d, *J* = 8.5 Hz, 1H), 7.11 (t, *J* = 7.5 Hz, 1H), 6.85 (d, *J* = 7.9 Hz, 1H), 6.68 (t, *J* = 7.9 Hz, 1H), 6.44 (d, *J* = 7.9 Hz, 1H), 5.99 (s, 1H), 5.95 (s, 1H), 3.59 (s, 3H), 3.29 (s, 3H). ^{13}C NMR (125 MHz, DMSO-d_6): δ = 154.8, 153.3, 152.9, 150.9, 147.7, 147.2, 144.6, 131.2, 129.5, 126.9, 122.6, 121.4, 120.8, 119.9, 112.9, 110.3, 108.5, 106.7, 101.1, 99.0, 55.7, 28.8. IR (film): $\tilde{\nu}$ = 3520, 3151, 3000, 2822, 1667, 1600, 1507, 1438, 1025, 739 cm^{-1}. HRMS (ESI), *m*/*z*: calcd for $C_{22}H_{17}N_5NaO_5$, 454.1127; found, 454.1113 [M + Na]$^+$.

8-(Butyl)-1-methyl-7-*o*-methoxyphenyl-1*H*-imidazo[2,1-*f*]purine-2,4(3*H*,8*H*)-dione (51). White solid. Yield: 28%. Mp 242−244 °C. ^{1}H NMR (500 MHz, DMSO-d_6): δ = 10.89 (s, 1H), 7.53 (t, *J* = 7.8 Hz, 1H), 7.50 (s, 1H), 7.38 (d, *J* = 7.8 Hz, 1H), 7.19 (d, *J* = 7.8 Hz, 1H), 7.08 (t, *J* = 7.8 Hz, 1H), 3.84 (t, *J* = 7.3 Hz, 2H), 3.81 (s, 3H), 3.39 (s, 3H), 1.60 (quint, *J* = 7.3 Hz, 2H), 1.08 (sext, *J* = 7.3 Hz, 2H), 0.69 (t, *J* = 7.3 Hz, 3H). ^{13}C NMR (125 MHz, DMSO-d_6): δ = 157.3, 153.2, 152.7, 150.9, 147.3, 132.3, 131.5, 129.0, 120.6, 116.3, 111.4, 105.3, 98.8, 55.4, 43.4, 29.9, 28.8, 18.8, 12.9. IR (film): $\tilde{\nu}$ = 3145, 2999, 2934, 2837, 1674, 1514, 1461, 1246, 745 cm^{-1}. HRMS (ESI), *m*/*z*: calcd for $C_{19}H_{21}N_5NaO_3$, 390.1542; found, 390.1545 [M + Na]$^+$.

8-(Butyl)-1-methyl-7-*m*-methoxyphenyl-1*H*-imidazo[2,1-*f*]purine-2,4(3*H*,8*H*)-dione (52). White solid. Yield: 52%. Mp 206−208 °C. ^{1}H NMR (500 MHz, DMSO-d_6): δ = 10.91 (s, 1H), 7.70 (s, 1H), 7.44 (t, *J* = 8.2 Hz, 1H), 7.13−7.14 (m, 2H), 7.05 (dd, *J* = 8.2, 2.4 Hz, 1H), 4.11 (t, *J* = 7.3 Hz, 2H), 3.82 (s, 3H), 3.39 (s, 3H), 1.63 (quint, *J* = 7.3 Hz, 2H), 1.13 (sext, *J* = 7.3 Hz, 2H), 0.74 (t, *J* = 7.3 Hz, 3H). ^{13}C NMR (125 MHz, DMSO-d_6): δ = 159.4, 153.2, 152.7, 150.9, 147.9, 132.0, 130.0, 129.2, 120.8, 114.8, 114.1, 105.2, 98.8, 55.2, 43.5, 30.2, 28.8, 18.9, 13.1. IR (film): $\tilde{\nu}$ = 3141, 3044, 2957, 2817, 1679, 1509, 1467, 1156, 716 cm^{-1}. HRMS (ESI), *m*/*z*: calcd for $C_{19}H_{21}N_5NaO_3$, 390.1542; found, 390.1544 [M + Na]$^+$.

8-(Butyl)-1-methyl-7-*p*-methoxyphenyl-1*H*-imidazo[2,1-*f*]purine-2,4(3*H*,8*H*)-dione (53). White solid. Yield: 89%. Mp 272−274 °C. ^{1}H NMR (500 MHz, DMSO-d_6): δ = 10.90 (s, 1H), 7.60 (s, 1H), 7.51 (d, *J* = 8.7 Hz, 2H), 7.09 (d, *J* = 8.7 Hz, 2H), 4.07 (t, *J* = 7.3 Hz, 2H), 3.83 (s, 3H), 3.40 (s, 3H), 1.62 (quint, *J* = 7.3 Hz, 2H), 1.12 (sext, *J* = 7.3 Hz, 2H), 0.75 (t, *J* = 7.3 Hz, 3H). IR (film): $\tilde{\nu}$ = 3144, 3051, 2963, 2864, 2802, 1671, 1507, 1247, 831, 742 cm^{-1}. HRMS (ESI), *m*/*z*: calcd for $C_{19}H_{21}N_5NaO_3$, 390.1542; found, 390.1541 [M + Na]$^+$.

8-(2-Methoxyphenyl)-1-methyl-7-*o*-methylphenyl-1*H*-imidazo-[2,1-*f*]purine-2,4(3*H*,8*H*)-dione (54). White solid. Yield: 64%. Mp 301−303 °C. ^{1}H NMR (400 MHz, DMSO-d_6): δ = 10.98 (s, 1H), 7.81 (s, 1H), 7.49 (dd, *J* = 7.7, 1.6 Hz, 1H), 7.39 (ddd, *J* = 8.6, 8.3, 1.6 Hz, 1H), 7.21−7.22 (m, 2H), 7.13−7.15 (m, 1H), 7.04−7.08 (m, 2H), 7.00 (ddd, *J* = 8.6, 7.7, 1.2 Hz, 1H), 3.57 (s, 3H), 3.31 (s, 3H), 2.27 (s, 3H). ^{13}C NMR (100 MHz, DMSO-d_6): δ = 154.8, 153.3, 152.9, 150.9, 147.7, 147.2, 144.6, 131.2, 129.5, 126.9, 122.6, 121.4, 120.8, 119.9, 112.9, 110.3, 108.5, 106.7, 101.1, 99.0, 55.7, 28.8. IR (film): $\tilde{\nu}$ = 3166, 3007, 2811, 1666, 1490, 1157, 744 cm^{-1}. HRMS (ESI), *m*/*z*: calcd for $C_{22}H_{19}N_5NaO_3$, 424.1386; found, 424.1389 [M + Na]$^+$.

8-(2-Methoxyphenyl)-1-methyl-7-*m*-methylphenyl-1*H*-imidazo-[2,1-*f*]purine-2,4(3*H*,8*H*)-dione (55). White solid. Yield: 72%. Mp 313−315 °C. ^{1}H NMR (500 MHz, DMSO-d_6): δ = 10.98

(s, 1H), 7.95 (s, 1H), 7.51 (d, J = 7.2 Hz, 2H), 6.98−7.21 (m, 6H), 3.58 (s, 3H), 3.30 (s, 3H), 2.20 (s, 3H). ^{13}C NMR (125 MHz, DMSO-d_6): δ = 154.9, 153.3, 152.7, 150.9, 147.9, 137.5, 133.0, 131.2, 129.8, 128.9, 128.2, 128.1, 128.0, 124.3, 122.6, 120.9, 112.9, 105.2, 99.1, 55.7, 28.8, 20.8. IR (film): $\tilde{\nu}$ = 3160, 3028, 2822, 1704, 1671, 1505, 1435, 1160, 738 cm^{-1}. HRMS (ESI), m/z: calcd for $C_{22}H_{19}N_5NaO_3$, 424.1386; found, 424.1383 [M + Na]$^+$.

8-(Butyl)-1-methyl-7-*m*-methylphenyl-1*H*-imidazo[2,1-*f*]purine-2,4(3*H*,8*H*)-dione (56). White solid. Yield: 42%. Mp 238−240 °C. ^{1}H NMR (500 MHz, DMSO-d_6): δ = 10.91 (s, 1H), 7.65 (s, 1H), 7.40−7.43 (m, 2H), 7.37 (d, J = 7.6 Hz, 1H), 7.31 (d, J = 7.6 Hz, 1H), 4.10 (t, J = 7.3 Hz, 2H), 3.40 (s, 3H), 2.38 (s, 3H), 1.62 (quint, J = 7.3 Hz, 2H), 1.12 (sext, J = 7.3 Hz, 2H), 0.74 (t, J = 7.3 Hz, 3H). ^{13}C NMR (125 MHz, DMSO-d_6): δ = 153.2, 152.7, 150.9, 147.9, 138.3, 132.3, 129.6, 129.3, 128.8, 127.9, 125.8, 104.9, 98.8, 43.3, 30.1, 28.8, 20.8, 18.8, 13.0. IR (film): $\tilde{\nu}$ = 3160, 3044, 2949, 2802, 1672, 1509, 1147, 721 cm^{-1}. HRMS (ESI), m/z: calcd for $C_{19}H_{21}N_5NaO_2$, 374.1593; found, 374.1584 [M + Na]$^+$.

8-(Butyl)-1-methyl-7-*p*-methylphenyl-1*H*-imidazo[2,1-*f*]purine-2,4(3*H*,8*H*)-dione (57). White solid. Yield: 24%. Mp 227−229 °C. ^{1}H NMR (500 MHz, DMSO-d_6): δ = 10.91 (s, 1H), 7.63 (s, 1H), 7.46 (d, J = 7.9 Hz, 2H), 7.34 (d, J = 7.9 Hz, 2H), 4.09 (t, J = 7.3 Hz, 2H), 3.40 (s, 3H), 2.38 (s, 3H), 1.62 (quint, J = 7.3 Hz, 2H), 1.11 (sext, J = 7.3 Hz, 2H), 0.74 (t, J = 7.3 Hz, 3H). ^{13}C NMR (125 MHz, DMSO-d_6): δ = 153.2, 152.7, 150.9, 147.8, 138.6, 132.2, 129.5, 128.8, 125.0, 104.7, 98.8, 43.3, 30.2, 28.8, 20.7, 18.8, 13.1. IR (film): $\tilde{\nu}$ = 3169, 3051, 2958, 2858, 2785, 1671, 1506, 1294, 1147, 825 cm^{-1}. HRMS (ESI), m/z: calcd for $C_{19}H_{21}N_5NaO_2$, 374.1593; found, 374.1589 [M + Na]$^+$.

8-(2-Methoxyphenyl)-1-methyl-7-*o*-hydroxyphenyl-1*H*-imidazo-[2,1-*f*]purine-2,4(3*H*,8*H*)-dione (58). Yellow solid. Yield: 50%. Mp 350−352 °C. ^{1}H NMR (500 MHz, DMSO-d_6): δ = 10.95 (s, 1H), 9.75 (s, 1H), 7.68 (s, 1H), 7.40−7.44 (m, 2H), 7.10−7.14 (m, 2H), 7.00−7.04 (m, 2H), 6.81 (dd, J = 8.2, 0.9 Hz, 1H), 6.67 (ddd, J = 8.4, 7.5, 0.9 Hz, 1H), 3.58 (s, 3H), 3.30 (s, 3H). ^{13}C NMR (125 MHz, DMSO-d_6): δ = 155.5, 154.8, 153.3, 152.7, 150.9, 147.5, 130.7, 130.6, 130.1, 129.7, 129.4, 122.8, 120.5, 118.3, 115.5, 114.7, 112.7, 106.4, 98.9, 55.5, 28.7. IR (film): $\tilde{\nu}$ = 3251, 3166, 2821, 1677, 1486, 1445, 1159, 744 cm^{-1}. HRMS (ESI), m/z: calcd for $C_{21}H_{17}N_5NaO_4$, 426.1178; found, 426.1174 [M + Na]$^+$.

8-(Butyl)-1-methyl-7-*o*-hydroxyphenyl-1*H*-imidazo[2,1-*f*]purine-2,4(3*H*,8*H*)-dione (59). White solid. Yield: 22%. Mp 209−211 °C. ^{1}H NMR (400 MHz, DMSO-d_6): δ = 10.88 (s, 1H), 9.99 (s, 1H), 7.48 (s, 1H), 7.35 (t, J = 7.8 Hz, 1H), 7.30 (d, J = 7.8 Hz, 1H), 7.00 (d, J = 7.8 Hz, 1H), 6.93 (t, J = 7.8 Hz, 1H), 3.92 (t, J = 7.3 Hz, 2H), 3.40 (s, 3H), 1.60 (quint, J = 7.3 Hz, 2H), 1.08 (sext, J = 7.3 Hz, 2H), 0.70 (t, J = 7.3 Hz, 3H). ^{13}C NMR (100 MHz, DMSO-d_6): δ = 155.8, 153.2, 152.6, 150.9, 147.4, 132.2, 131.2, 129.6, 119.2, 115.7, 114.8, 105.1, 98.8, 43.4, 30.1, 28.8, 18.8, 13.0. IR (film): $\tilde{\nu}$ = 3138, 3044, 2953, 2870, 2811, 1683, 1509, 1200, 739 cm^{-1}. HRMS (ESI), m/z: calcd for $C_{18}H_{19}N_5NaO_3$, 376.1386; found, 376.1383 [M + Na]$^+$.

8-(2-Methoxyphenyl)-1-methyl-7-*m*-hydroxyphenyl-1*H*-imidazo-[2,1-*f*]purine-2,4(3*H*,8*H*)-dione (60). White solid. Yield: 59%. Mp 353−355 °C. ^{1}H NMR (500 MHz, DMSO-d_6): δ = 10.97 (s, 1H), 9.51 (s, 1H), 7.88 (s, 1H), 7.47−7.52 (m, 2H), 7.20 (d, J = 8.2 Hz, 1H), 7.06−7.11 (m, 2H), 6.68−6.70 (m, 2H), 6.64 (s, 1H), 3.60 (s, 3H), 3.29 (s, 3H). ^{13}C NMR (125 MHz, DMSO-d_6): δ = 157.1, 154.9, 153.3, 152.7, 150.9, 147.9, 133.1, 131.1, 129.7, 129.4, 129.2, 122.6, 120.9, 118.3, 115.4, 114.4, 112.9, 105.1, 99.1, 55.7, 28.8. IR (film): $\tilde{\nu}$ = 3147, 3030, 2817, 1676, 1482, 1299, 1159, 758 cm^{-1}. HRMS (ESI), m/z: calcd for $C_{21}H_{17}N_5NaO_4$, 426.1178; found, 426.1181 [M + Na]$^+$.

8-(Butyl)-1-methyl-7-*m*-hydroxyphenyl-1*H*-imidazo[2,1-*f*]purine-2,4(3*H*,8*H*)-dione (61). White solid. Yield: 41%. Mp 256−258 °C. ^{1}H NMR (500 MHz, DMSO-d_6): δ = 10.89 (s, 1H), 9.75 (s, 1H), 7.59 (s, 1H), 7.31 (t, J = 7.8 Hz, 1H), 6.96 (d, J = 7.8 Hz, 1H), 6.93 (s, 1H), 6.88 (d, J = 7.8 Hz, 1H), 4.07 (t, J = 7.3 Hz, 2H), 3.38 (s, 3H), 1.63 (quint, J = 7.3 Hz, 2H), 1.12 (sext, J = 7.3 Hz, 2H), 0.74 (t, J = 7.3 Hz, 3H). ^{13}C NMR (125 MHz, DMSO-d_6): δ = 157.6, 153.2, 152.7, 150.9, 147.8, 132.3, 129.9, 129.0, 119.5, 116.0, 115.6, 104.7, 98.8, 43.3, 30.2, 28.8, 18.8, 13.1. IR (film): $\tilde{\nu}$ = 3297, 3166, 3046, 2963, 2864, 1675, 1512, 1459, 1312, 1148, 722 cm^{-1}. HRMS (ESI), m/z: calcd for $C_{18}H_{19}N_5NaO_3$, 376.1386; found, 376.1388 [M + Na]$^+$.

8-(2-Methoxyphenyl)-1-methyl-7-*p*-hydroxyphenyl-1*H*-imidazo-[2,1-*f*]purine-2,4(3*H*,8*H*)-dione (62). White solid. Yield: 3%. Mp 364−366 °C. ^{1}H NMR (500 MHz, DMSO-d_6): δ = 10.94 (s, 1H), 9.66 (s, 1H), 7.78 (s, 1H), 7.50 (ddd, J = 8.4, 7.6, 1.7 Hz, 1H), 7.47 (dd, J = 7.7, 1.7 Hz, 1H), 7.19 (dd, J = 8.4, 1.1 Hz, 1H), 7.05−7.10 (m, 3H), 6.65 (d, J = 8.7 Hz, 2H), 3.60 (s, 3H), 3.29 (s, 3H). ^{13}C NMR (125 MHz, DMSO-d_6): δ = 157.6, 155.0, 153.3, 152.5, 150.9, 147.7, 133.4, 131.1, 129.9, 129.2, 122.6, 120.9, 118.7, 115.1, 112.9, 104.1, 99.0, 55.7, 28.7. IR (film): $\tilde{\nu}$ = 3326, 3140, 3005, 2820, 1678, 1508, 1438, 1226, 1159, 838, 742 cm^{-1}. HRMS (ESI), m/z: calcd for $C_{21}H_{17}N_5NaO_4$, 426.1178; found, 426.1177 [M + Na]$^+$.

8-(Butyl)-1-methyl-7-*p*-hydroxyphenyl-1*H*-imidazo[2,1-*f*]purine-2,4(3*H*,8*H*)-dione (63). White solid. Yield: 10%. Mp 277−281 °C. ^{1}H NMR (400 MHz, DMSO-d_6): δ = 10.89 (s, 1H), 9.85 (s, 1H), 7.52 (s, 1H), 7.36 (d, J = 8.7 Hz, 2H), 6.89 (d, J = 8.7 Hz, 2H), 4.04 (t, J = 7.3 Hz, 2H), 3.39 (s, 3H), 1.62 (quint, J = 7.3 Hz, 2H), 1.12 (sext, J = 7.3 Hz, 2H), 0.74 (t, J = 7.3 Hz, 3H). ^{13}C NMR (100 MHz, DMSO-d_6): δ = 158.2, 153.2, 152.6, 150.9, 147.6, 132.5, 130.5, 118.3, 115.6, 104.1, 98.8, 43.1, 30.2, 28.8, 18.8, 13.1. IR (film): $\tilde{\nu}$ = 3283, 3160, 3043, 2973, 1676, 1510, 1226, 1148, 843, 716 cm^{-1}. HRMS (ESI), m/z: calcd for $C_{18}H_{19}N_5NaO_3$, 376.1386; found, 376.1381 [M + Na]$^+$.

8-(2-Methoxyphenyl)-1-methyl-7-(2′-methyl-3′-hydroxyphenyl-1*H*-imidazo[2,1-*f*]purine-2,4(3*H*,8*H*)-dione (64). Light-yellow solid. Yield: 56%. Mp 372−374 °C. ^{1}H NMR (400 MHz, DMSO-d_6): δ = 10.96 (s, 1H), 9.43 (s, 1H), 7.71 (s, 1H), 7.38−7.42 (m, 2H), 7.09 (d, J = 8.1 Hz, 1H), 6.99 (t, J = 7.6 Hz, 1H), 6.89 (t, J = 7.6 Hz, 1H), 6.75 (d, J = 8.1 Hz, 1H), 6.64 (d, J = 7.6 Hz, 1H), 3.60 (s, 3H), 3.30 (s, 3H), 2.01 (s, 3H). ^{13}C NMR (100 MHz, DMSO-d_6): δ = 155.1, 154.7, 153.3, 152.7, 150.9, 147.4, 132.1, 130.8, 129.6, 128.3, 125.4, 124.5, 122.2, 121.9, 120.5, 115.3, 112.5, 106.1, 99.0, 55.5, 28.7, 12.9. IR (film): $\tilde{\nu}$ = 3326, 3145, 3062, 2963, 2817, 1669, 1508, 1280, 1157, 747 cm^{-1}. HRMS (ESI), m/z: calcd for $C_{22}H_{19}N_5NaO_4$, 440.1335; found, 440.1332 [M + Na]$^+$.

8-(2-Methoxyphenyl)-1-methyl-7-(2′-methyl-4′-hydroxyphenyl-1*H*-imidazo[2,1-*f*]purine-2,4(3*H*,8*H*)-dione (65). White solid. Yield: 52%. Mp 330−333 °C. ^{1}H NMR (400 MHz, DMSO-d_6): δ = 10.94 (s, 1H), 9.55 (s, 1H), 7.66 (s, 1H), 7.38−7.43 (m, 2H), 7.09 (d, J = 7.5 Hz, 1H), 7.00 (t, J = 7.5 Hz, 1H), 6.94 (d, J = 8.3 Hz, 1H), 6.57 (s, 1H), 6.44 (d, J = 8.3 Hz, 1H), 3.60 (s, 3H), 3.30 (s, 3H), 2.14 (s, 3H). IR (film): $\tilde{\nu}$ = 3208, 3048, 2942, 2838, 1675, 1596, 1455, 1205, 1153, 747 cm^{-1}. HRMS (ESI), m/z: calcd for $C_{22}H_{19}N_5NaO_4$, 440.1335; found, 440.1330 [M + Na]$^+$.

8-(2-Methoxyphenyl)-1-methyl-7-(2′-methyl-5′-hydroxyphenyl-1*H*-imidazo[2,1-*f*]purine-2,4(3*H*,8*H*)-dione (66). White solid. Yield: 45%. Mp 350−352 °C. ^{1}H NMR (400 MHz, DMSO-d_6): δ = 10.96 (s, 1H), 9.22 (s, 1H), 7.74 (s, 1H), 7.39−7.44 (m, 2H), 7.10 (dd, J = 8.4, 0.9 Hz, 1H), 6.97−7.04 (m, 2H), 6.62 (dd, J = 8.3, 2.6 Hz, 1H), 6.56 (d, J = 2.6 Hz, 1H), 3.61 (s, 3H), 3.30 (s, 3H), 2.12 (s, 3H). ^{13}C NMR (100 MHz, DMSO-d_6): δ = 154.6, 154.4, 153.3, 152.7, 150.9, 147.4, 131.8, 130.8, 130.7, 129.5, 127.8, 127.6, 122.2, 120.5, 117.7, 116.2, 112.6, 106.1, 99.0, 55.5, 28.7, 18.6. IR (film): $\tilde{\nu}$ = 3296, 3145, 1698, 1670, 1593, 1505, 1282, 1153, 1017, 751 cm^{-1}. HRMS (ESI), m/z: calcd for $C_{22}H_{19}N_5NaO_4$, 440.1335; found, 440.1333 [M + Na]$^+$.

8-(2-Methoxyphenyl)-1-methyl-7-(2′,5′-dihydroxyphenyl-1*H*-imidazo[2,1-*f*]purine-2,4(3*H*,8*H*)-dione (67). White solid. Yield: 34%. Mp 333−336 °C. ^{1}H NMR (400 MHz, DMSO-d_6): δ = 10.94 (s, 1H), 9.18 (s, 1H), 8.96 (s, 1H), 7.69 (s, 1H), 7.50 (t, J = 7.6 Hz, 1H), 7.42 (d, J = 7.6 Hz, 1H), 7.20 (d, J = 7.6 Hz, 1H), 7.07 (t, J = 7.6 Hz, 1H), 6.61−6.63 (m, 2H), 6.53 (dd, J = 7.8, 1.8 Hz,

1H), 3.64 (s, 3H), 3.28 (s, 3H). ^{13}C NMR (100 MHz, DMSO-d_6): δ = 155.1, 153.3, 152.5, 150.9, 147.7, 145.9, 144.9, 133.7, 131.1, 129.9, 122.7, 120.8, 119.4, 118.9, 115.4, 115.3, 112.9, 103.9, 99.0, 55.7, 28.8. IR (film): $\tilde{\nu}$ = 3446, 3243, 3062, 1714, 1656, 1506, 1464, 1276, 1148, 749 cm^{-1}. HRMS (ESI), *m*/*z*: calcd for $C_{21}H_{17}N_5NaO_5$, 442.1121; found, 442.1122 [M + Na]$^+$.

8-(2-Methoxyphenyl)-1-methyl-7-*p*-cyanophenyl-1*H*-imidazo-[2,1-*f*]purine-2,4(3*H*,8*H*)-dione (68). White solid. Yield: 68%. Mp 303−305 °C. ^{1}H NMR (400 MHz, DMSO-d_6): δ = 11.04 (s, 1H), 8.28 (s, 1H), 7.77 (d, *J* = 8.4 Hz, 2H), 7.62 (dd, *J* = 7.6, 1.2 Hz, 1H), 7.55 (dt, *J* = 7.6, 1.2 Hz, 1H), 7.43 (d, *J* = 8.4 Hz, 2H), 7.20 (dd, *J* = 7.6, 1.2 Hz, 1H), 7.15 (dt, *J* = 7.6, 1.2 Hz, 1H), 3.53 (s, 3H), 3.30 (s, 3H). ^{13}C NMR (100 MHz, DMSO-d_6): δ = 154.4, 153.3, 153.1, 150.9, 148.3, 132.9, 132.3, 131.5, 131.1, 129.5, 127.4, 122.2, 121.2, 118.3, 113.1, 110.5, 107.2, 99.2, 55.6, 28.8. IR (film): $\tilde{\nu}$ = 3010, 2835, 1680, 1497, 745, 605, 445 cm^{-1}. HRMS (ESI), *m*/*z*: calcd for $C_{22}H_{16}N_6NaO_3$, 435.1182; found, 435.1187 [M + Na]$^+$.

7-*p*-Fluorophenyl-8-(2-methoxyphenyl)-1*H*-imidazo[2,1-*f*]purine-2,4(3*H*,8*H*)-dione (69). A mixture of **46** (528 mg, 1.09 mmol), 10% Pd−C (339 mg), and dry ammonium formate (692 mg, 10.9 mmol) in absolute methanol (16 mL) was heated in a sealed tube at 140 °C for 3 h. The mixture was cooled to room temperature, and the mixture was filtered over a short path of Celite. The residue was evaporated under reduced pressure, affording the desired compound as a white solid (121 mg, 28% yield). Mp 330−333 °C. ^{1}H NMR (400 MHz, DMSO-d_6): δ = 11.53 (s, 1H), 10.71 (s, 1H), 7.96 (s, 1H), 7.47−7.51 (m, 2H), 7.28−7.31 (m, 2H), 7.13−7.18 (m, 3H), 7.06−7.10 (m, 1H), 3.56 (s, 3H). ^{13}C NMR (100 MHz, DMSO-d_6): δ = 162.4 (d, *J* = 246.1 Hz), 155.2, 154.7, 152.7, 151.7, 148.9, 132.3, 131.7, 130.2 (d, *J* = 8.4 Hz), 130.1, 125.3 (d, *J* = 3.2 Hz), 122.9, 121.4, 115.9 (d, *J* = 21.8 Hz), 113.4, 105.9, 99.5, 56.2. IR (film): $\tilde{\nu}$ = 3159, 2900, 1668, 1500, 1393, 1242, 1065, 750, 536 cm^{-1}. MS (ESI), *m*/*z*: calcd for $C_{20}H_{14}FN_5NaO_3$: 414.3; found, 414.2 [M + Na]$^+$.

8-(2-Methoxyphenyl)-1-methyl-7-*p*-carboxyphenyl-1*H*-imidazo-[2,1-*f*]purine-2,4(3*H*,8*H*)-dione (70). To a solution of 8-(2-methoxyphenyl)-1-methyl-7-*p*-cyanophenyl-1*H*-imidazo[2,1-*f*]purine-2,4(3*H*,8*H*)-dione (**68**, 85 mg, 0.206 mmol) in water (0.910 mL) was added concentrated H_2SO_4 (0.803 mL), and the mixture was refluxed for 2 h. The mixture was cooled to room temperature, water (1 mL) was added, and the precipitate formed was filtered off, affording the desired product as a white solid (60 mg, 67% yield). ^{1}H NMR (400 MHz, DMSO-d_6): δ = 11.02 (s, 1H), 8.16 (s, 1H), 7.82 (d, *J* = 8.3 Hz, 2H), 7.58 (dd, *J* = 7.7, 1.4 Hz, 1H), 7.53 (dt, *J* = 7.7, 1.4 Hz, 1H), 7.37 (d, *J* = 8.3 Hz, 2H), 7.19 (d, *J* = 7.6 Hz, 1H), 7.14 (t, *J* = 7.6 Hz, 1H), 3.54 (s, 3H), 3.30 (s, 3H), CO_2H not observed. ^{13}C NMR (100 MHz, DMSO-d_6): δ = 166.6, 154.6, 153.3, 152.9, 150.9, 148.2, 132.4, 131.9, 131.3, 130.3, 129.6, 129.2, 127.0, 122.4, 121.1, 113.0, 106.4, 99.1, 55.6, 28.8. IR (film): $\tilde{\nu}$ = 3013, 2839, 1681, 1547, 1264, 1158, 1013, 745, 570 cm^{-1}. HRMS (ESI), *m*/*z*: calcd for $C_{22}H_{17}N_5NaO_5$, 454.1127; found, 454.1135 [M + Na]$^+$. HPLC purity 88%.

FRET Based Enzymatic Assay. Compounds were tested in the Z'-LYTE kinase assay kit—Tyr 1 peptide (Invitrogen, USA) in a Corning 384-well microtiter plate. Fluorescence progress curves were measured upon excitation at 400 nm and emission at 445 and 520 nm. The assay contained a final concentration of EphB4 and ATP of 25 ng/μL and 125 μM (which is near its K_m), respectively, and was run at 30 °C for 2 h. IC_{50} values (inhibitor concentration at which enzyme activity is reduced by 50%) are determined after carrying out assays at 10 different concentrations between 20 μM and 10 pM.

[γ-^{33}P]ATP Based Enzymatic Assay. The enzymatic assays of selectivity profile were performed in Reaction Biology Corporation and the National Centre for Protein Kinase Profiling of University Dundee. All assays (25.5 μL volume) performed at the University of Dundee were carried out robotically at room temperature and were linear with respect to time and enzyme concentration under the conditions used. Assays were performed for 30 min using Multidrop Micro reagent dispensers (Thermo Electron Corporation, Waltham, MA) in a 96-well format. The concentration of magnesium acetate in the assays was 10 mM, and [γ-^{33}P]ATP (800 cpm/pmol) was used at 5, 20, or 50 μM as indicated in Supporting Information, in order to be at or below the K_m for ATP for each kinase. The assays were initiated with MgATP, stopped by the addition of 5 μL of 0.5 M orthophosphoric acid, and spotted on to P81 filter plates using a unifilter harvester (PerkinElmer, Boston, MA). IC_{50} values were determined after carrying out assays at 10 different concentrations between 10 μM and 110 pM. The data are presented as mean percentage activity of duplicate assays at single concentration compared to DMSO controls. A similar protocol was used at Reaction Biology Corporation to measure the inhibitory activity of compound **66** against 11 Eph kinases.

Phage Display Based Binding Assay. The experiments were performed at Ambit Biosciences Corporation using binding assays as previously described.[11] Briefly, kinases were expressed as fusion proteins to T7 phage. In general, full-length constructs were used for small kinases and catalytic domains for large kinases. T7-kinase-tagged phage strains were mixed with known kinase inhibitors immobilized on streptavidin-coated magnetic beads and with test compounds at a single concentration of 1 μM. Test compounds that bind to the kinase ATP site displace the immobilized ligand from the kinase/phage, which is detected using quantitative PCR. The results are reported as the percentage of kinase/phage remaining bound to the ligand/beads, relative to a control (DMSO lacking a test compound). High affinity compounds have % control = 0, while weaker binders have higher % control values. Results are reported for screening against 50 human kinases.

Acknowledgment. We thank Marino Convertino and Dr. Peter Kolb for interesting discussions. The calculations were performed on the Matterhorn Beowulf cluster at the Informatikdienste of the University of Zurich. This work was supported in part by a grant of the Swiss National Science Foundation to A.C. and the Organic Chemistry Institute of the University of Zurich to C.N.

Supporting Information Available: Biological activity of compounds **54** and **66** on the selected kinases, conformation analysis data, times series of van der Waals and electrostatic interaction energies, SAR-based dendrogram, experimental protocols for **5**−**14**, and analytical data for final compounds **45**−**70** and intermediates **5**−**14**, **16**−**18**, and **21**−**44**. This material is available free of charge via the Internet at http://pubs.acs.org.

References

(1) Folkman, J. Angiogenesis in cancer, vascular, rheumatoid and other disease. *Nat. Med* **1995**, *1*, 27–31.
(2) Folkman, J. Tumor angiogenesis: therapeutic implications. *N. Engl. J. Med.* **1971**, *285*, 1182–1186.
(3) Adams, R. H. Vascular patterning by Eph receptor tyrosine kinases and ephrins. *Semin. Cell Dev. Biol.* **2002**, *13*, 55–60.
(4) Martiny-Baron, G.; Korff, T.; Schaffner, F.; Esser, N.; Eggstein, S.; Marme, D.; Augustin, H. G. Inhibition of tumor growth and angiogenesis by soluble EphB4. *Neoplasia* **2004**, *6*, 248–257.
(5) Kertesz, N.; Krasnoperov, V.; Reddy, R.; Leshanski, L.; Kumar, S. R.; Zozulya, S.; Gill, P. S. The soluble extracellular domain of EphB4 (sEphB4) antagonizes EphB4−EphrinB2 interaction, modulates angiogenesis, and inhibits tumor growth. *Blood* **2006**, *107*, 2330–2338.
(6) Kolb, P.; Kipouros, C. B.; Huang, D.; Caflisch, A. Structure-based tailoring of compound libraries for high-throughput screening: discovery of novel EphB4 kinase inhibitors. *Proteins* **2008**, *73*, 11–18.
(7) Miyazaki, Y.; Nakano, M.; Sato, H.; Truesdale, A. T.; Stuart, J. D.; Nartey, E. N.; Hightower, K. E.; Kane-Carson, L. Design and effective synthesis of novel templates, 3,7-diphenyl-4-aminothieno and furo-[3,2-*c*]pyridines as protein kinase inhibitors and

in vitro evaluation targeting angiogenetic kinases. *Bioorg. Med. Chem. Lett.* **2007**, *17*, 250–254.
(8) Bardelle, C.; Cross, D.; Davenport, S.; Kettle, J. G.; Ko, E. J.; Leach, A. G.; Mortlock, A.; Read, J.; Roberts, N. J.; Robins, P.; Williams, E. J. Inhibitors of the tyrosine kinase EphB4. Part 1: Structure-based design and optimization of a series of 2,4-bis-anilinopyrimidines. *Bioorg. Med. Chem. Lett.* **2008**, *18*, 2776–2780.
(9) Sun, L.; Liang, C.; Shirazian, S.; Zhou, Y.; Miller, T.; Cui, J.; Fukuda, J. Y.; Chu, J. Y.; Nematalla, A.; Wang, X. Y.; Chen, H.; Sistla, A.; Luu, T. C.; Tang, F.; Wei, J.; Tang, C. Discovery of 5-[5-fluoro-2-oxo-1,2-dihydroindol-(3*Z*)-ylidenemethyl]-2,4-dimethyl-1*H*-pyrrole-3-carboxylic acid (2-diethylaminoethyl)amide, a novel tyrosine kinase inhibitor targeting vascular endothelial and platelet-derived growth factor receptor tyrosine kinase. *J. Med. Chem.* **2003**, *46*, 1116–1119.
(10) Bardelle, C.; Coleman, T.; Cross, D.; Davenport, S.; Kettle, J. G.; Ko, E. J.; Leach, A. G.; Mortlock, A.; Read, J.; Roberts, N. J.; Robins, P.; Williams, E. J. Inhibitors of the tyrosine kinase EphB4. Part 2: Structure-based discovery and optimisation of 3,5-bis substituted anilinopyrimidines. *Bioorg. Med. Chem. Lett.* **2008**, *18*, 5717–5721.
(11) Karaman, M. W.; Herrgard, S.; Treiber, D. K.; Gallant, P.; Atteridge, C. E.; Campbell, B. T.; Chan, K. W.; Ciceri, P.; Davis, M. I.; Edeen, P. T.; Faraoni, R.; Floyd, M.; Hunt, J. P.; Lockhart, D. J.; Milanov, Z. V.; Morrison, M. J.; Pallares, G.; Patel, H. K.; Pritchard, S.; Wodicka, L. M.; Zarrinkar, P. P. A quantitative analysis of kinase inhibitor selectivity. *Nat. Biotechnol.* **2008**, *26*, 127–132.
(12) McInnes, C. Virtual screening strategies in drug discovery. *Curr. Opin. Chem. Biol.* **2007**, *11*, 494–502.
(13) Huang, D.; Caflisch, A. Library screening by fragment-based docking. *J. Mol. Recognit.*, DOI: 10.1002/jmr.981.
(14) Papesch, V.; Schroeder, E. F. Synthesis of 1-mono-substituted and 1,3-di-substituted 6-amino-uracils. Diuretic activity. *J. Org. Chem.* **1951**, *16*, 1879–1890.
(15) Merlos, M.; Gomez, L.; Vericat, M. L.; Bartroli, J.; Garciarafanell, J.; Forn, J. Structure−activity-relationships in a series of xanthine derivatives with antibronchoconstrictory and bronchodilatory activities. *Eur. J. Med. Chem.* **1990**, *25*, 653–658.
(16) Baraldi, P. G.; Preti, D.; Tabrizi, M. A.; Fruttarolo, F.; Romagnoli, R.; Zaid, N. A.; Moorman, A. R.; Merighi, S.; Varani, K.; Borea, P. A. New pyrrolo[2,1-*f*]purine-2,4-dione and imidazo[2,1-*f*]purine-2,4-dione derivatives as potent and selective human A3 adenosine receptor antagonists. *J. Med. Chem.* **2005**, *48*, 4697–4701.
(17) Traxler, P.; Furet, P. Strategies toward the design of novel and selective protein tyrosine kinase inhibitors. *Pharmacol. Ther.* **1999**, *82*, 195–206.
(18) Bamborough, P.; Angell, R. M.; Bhamra, I.; Brown, D.; Bull, J.; Christopher, J. A.; Cooper, A. W.; Fazal, L. H.; Giordano, I.; Hind, L.; Patel, V. K.; Ranshaw, L. E.; Sims, M. J.; Skone, P. A.; Smith, K. J.; Vickerstaff, E.; Washington, M. *N*-4-Pyrimidinyl-1*H*-indazol-4-amine inhibitors of Lck: indazoles as phenol isosteres with improved pharmacokinetics. *Bioorg. Med. Chem. Lett.* **2007**, *17*, 4363–4368.
(19) Huang, D.; Zhou, T.; Lafleur, K.; Nevado, C.; Caflisch, A. *Bioinformatics*, submitted.
(20) Bamborough, P.; Drewry, D.; Harper, G.; Smith, G. K.; Schneider, K. Assessment of chemical coverage of kinome space and its implications for kinase drug discovery. *J. Med. Chem.* **2008**, *51*, 7898–7914.
(21) Lombardo, L. J.; Lee, F. Y.; Chen, P.; Norris, D.; Barrish, J. C.; Behnia, K.; Castaneda, S.; Cornelius, L. A. M.; Das, J.; Doweyko, A. M.; Fairchild, C.; Hunt, J. T.; Inigo, I.; Johnston, K.; Kamath, A.; Kan, D.; Klei, H.; Marathe, P.; Pang, S. H.; Peterson, R.; Pitt, S.; Schieven, G. L.; Schmidt, R. J.; Tokarski, J.; Wen, M. L.; Wityak, J.; Borzilleri, R. M. Discovery of *N*-(2-chloro-6-methylphenyl)-2-(6-(4-(2-hydroxyethyl)-piperazin-1-yl)-2-methylpyrimidin-4-ylamino)thiazole-5-carboxamide (BMS-354825), a dual Src/Abl kinase inhibitor with potent antitumor activity in preclinical assays. *J. Med. Chem.* **2004**, *47*, 6658–6661.
(22) Hopkins, A. L.; Groom, C. R.; Alex, A. Ligand efficiency: a useful metric for lead selection. *Drug Discovery Today* **2004**, *9*, 430–431.
(23) Huang, D.; Luthi, U.; Kolb, P.; Cecchini, M.; Barberis, A.; Caflisch, A. In silico discovery of beta-secretase inhibitors. *J. Am. Chem. Soc.* **2006**, *128*, 5436–5443.
(24) Kolb, P.; Caflisch, A. Automatic and efficient decomposition of two-dimensional structures of small molecules for fragment-based high-throughput docking. *J. Med. Chem.* **2006**, *49*, 7384–7392.
(25) Scarsi, M.; Apostolakis, J.; Caflisch, A. Continuum electrostatic energies of macromolecules in aqueous solutions. *J. Phys. Chem. A* **1997**, *101*, 8098–8106.
(26) Caflisch, A.; Fischer, S.; Karplus, M. Docking by Monte Carlo minimization with a solvation correction: application to an FKBP−substrate complex. *J. Comput. Chem.* **1997**, *18*, 723–743.
(27) Majeux, N.; Scarsi, M.; Apostolakis, J.; Ehrhardt, C.; Caflisch, A. Exhaustive docking of molecular fragments with electrostatic solvation. *Proteins* **1999**, *37*, 88–105.
(28) Majeux, N.; Scarsi, M.; Caflisch, A. Efficient electrostatic solvation model for protein-fragment docking. *Proteins* **2001**, *42*, 256–268.
(29) Budin, N.; Majeux, N.; Caflisch, A. Fragment-Based flexible ligand docking by evolutionary optimization. *Biol. Chem.* **2001**, *382*, 1365–1372.
(30) Cecchini, M.; Kolb, P.; Majeux, N.; Caflisch, A. Automated docking of highly flexible ligands by genetic algorithms: a critical assessment. *J. Comput. Chem.* **2004**, *25*, 412–422.
(31) Brooks, B. R.; Bruccoleri, R. E.; Olafson, B. D.; States, D. J.; Swaminathan, S.; Karplus, M. Charmm, a program for macromolecular energy, minimization, and dynamics calculations. *J. Comput. Chem.* **1983**, *4*, 187–217.
(32) Brooks, B. R.; Brooks, C. L., 3rd; Mackerell, A. D., Jr.; Nilsson, L.; Petrella, R. J.; Roux, B.; Won, Y.; Archontis, G.; Bartels, C.; Boresch, S.; Caflisch, A.; Caves, L.; Cui, Q.; Dinner, A. R.; Feig, M.; Fischer, S.; Gao, J.; Hodoscek, M.; Im, W.; Kuczera, K.; Lazaridis, T.; Ma, J.; Ovchinnikov, V.; Paci, E.; Pastor, R. W.; Post, C. B.; Pu, J. Z.; Schaefer, M.; Tidor, B.; Venable, R. M.; Woodcock, H. L.; Wu, X.; Yang, W.; York, D. M.; Karplus, M. CHARMM: the biomolecular simulation program. *J. Comput. Chem.* **2009**, *30*, 1545–1614.
(33) MacKerell, A. D.; Bashford, D.; Bellott, M.; Dunbrack, R. L.; Evanseck, J. D.; Field, M. J.; Fischer, S.; Gao, J.; Guo, H.; Ha, S.; Joseph-McCarthy, D.; Kuchnir, L.; Kuczera, K.; Lau, F. T. K.; Mattos, C.; Michnick, S.; Ngo, T.; Nguyen, D. T.; Prodhom, B.; Reiher, W. E.; Roux, B.; Schlenkrich, M.; Smith, J. C.; Stote, R.; Straub, J.; Watanabe, M.; Wiorkiewicz-Kuczera, J.; Yin, D.; Karplus, M. All-atom empirical potential for molecular modeling and dynamics studies of proteins. *J. Phys. Chem. B* **1998**, *102*, 3586–3616.
(34) Jorgensen, W. L.; Chandrasekhar, J.; Madura, J. D.; Impey, R. W.; Klein, M. L. Comparison of simple potential functions for simulating liquid water. *J. Chem. Phys.* **1983**, *79*, 926–935.
(35) Humphrey, W.; Dalke, A.; Schulten, K. VMD: visual molecular dynamics. *J. Mol. Graphics* **1996**, *14*, 33–38.
(36) Phillips, J. C.; Braun, R.; Wang, W.; Gumbart, J.; Tajkhorshid, E.; Villa, E.; Chipot, C.; Skeel, R. D.; Kale, L.; Schulten, K. Scalable molecular dynamics with NAMD. *J. Comput. Chem.* **2005**, *26*, 1781–1802.
(37) Essmann, U.; Perera, L.; Berkowitz, M. L.; Darden, T.; Lee, H.; Pedersen, L. G. A smooth particle mesh Ewald method. *J. Chem. Phys.* **1995**, *103*, 8577–8593.
(38) Martyna, G. J.; Tobias, D. J.; Klein, M. L. Constant-pressure molecular-dynamics algorithms. *J. Chem. Phys.* **1994**, *101*, 4177–4189.
(39) Feller, S. E.; Zhang, Y. H.; Pastor, R. W.; Brooks, B. R. Constant-pressure molecular-dynamics simulation. The Langevin piston method. *J. Chem. Phys.* **1995**, *103*, 4613–4621.
(40) Ryckaert, J. P.; Ciccotti, G.; Berendsen, H. J. C. Numerical-integration of Cartesian equations of motion of a system with constraints. Molecular-dynamics of *N*-alkanes. *J. Comput. Phys.* **1977**, *23*, 327–341.
(41) Ballester, P. J.; Richards, W. G. Ultrafast shape recognition to search compound databases for similar molecular shapes. *J. Comput. Chem.* **2007**, *28*, 1711–1723.
(42) Granovsky, A. A. *PC GAMESS/Firefly*, version 7.1.F. www http://classic.chem.msu.su/gran/gamess/index.html.
(43) Dumas, J.; Phillips, B.; Zhang, C.; Ladouceur, G. H.; Zhao, Q.; Hentemann, M.; Verma, S. K.; Zhu, Q.; Lavoie, R. C.; Fan, J. Benzofuran Derivatives Useful for Treating Hyper-Proliferative Disorders. WO/2005/014566, **2005**.
(44) Manning, G.; Whyte, D. B.; Martinez, R.; Hunter, T.; Sudarsanam, S. The protein kinase complement of the human genome. *Science* **2002**, *298*, 1912–1934.